Nonclassical coincidences of atomic and mechanical excitations

Alisa D. Manukhova ,* Andrey A. Rakhubovsky ,† and Radim Filip ‡
Department of Optics, Palacký University, 17. Listopadu 12, 771 46 Olomouc, Czech Republic

(Received 20 September 2022; accepted 6 August 2024; published 3 September 2024)

Hybrid systems hold promise to provide an advantage in future quantum technology. Operating such systems outside the classical regime is crucially important to fully realize their potential. We investigate a pulsed quantum nondemolition gate between a cloud of atoms and a mechanical oscillator in distant cavities and demonstrate that this gate is capable of producing nonclassical coincidences of excitations in the disparate subsystems interacting by light. The nonclassicality is justified by evaluation of excitations created simultaneously in both modes beyond any joint classical states of such subsystems. To test the result, we use a nonclassicality witness based on available homodyne tomography of the atomic and mechanical states. Using feasible parameters, we show that it is possible to turn the pulsed dynamics of the state-of-the-art systems into nonclassical coincidences, and illustrate it for the cases of the atom-light, optomechanical, and atom-mechanical hybrid interactions. These tests are necessary to open full investigation of quantum correlations in hybrid systems.

DOI: 10.1103/PhysRevResearch.6.033228

I. INTRODUCTION

In quantum physics, information is contained in quantum states irrespective of their carrier. In principle, this allows using the most suitable experimental platforms to demonstrate fundamental quantum phenomena and achieve challenging goals of quantum technology. Hybrid quantum systems [1–3] combining different continuous-variable (CV) and discrete-variable (DV) platforms can efficiently use the advantages of the various subsystems that form the whole [4,5]. In particular, the atom-mechanical hybrid systems can combine strong and well-developed quantum control of the atoms [6–8] to store quantum states with the benefits of mechanical oscillators [9]. The latter include high mechanical quality, inherent ability to couple to different wavelengths of radiation (e.g., both light and microwaves) and forces of different nature, and potential access to motional nonlinearities naturally inaccessible to the atoms [10].

The importance of the hybrid atom-mechanical systems is emphasized by the abundance of effort, both theoretical and experimental, in this direction (for an extensive review, see, e.g., Refs. [1–3,11] and references therein). Different strategies involve direct coupling of mechanical vibrations to the energy levels of the discrete-level system [12–16] or indirect coupling mediated by radiation [17,18]. In the latter approach, the subsystems do not have to be localized in the vicinity of each other, which offers a technological simplification and potentially allows coupling the systems that are very far away. A proposal to use light for coupling mechanical and atomic systems [19] was put forward a decade ago. Since then, significant experimental effort has been devoted to the implementation of a similar scheme [20–22], eventually reaching strong coherent coupling between the atoms and mechanical oscillator [23] and quantum atom-mechanical entanglement [24]. The next step in this direction is the implementation of basic pulsed hybrid gates between atoms and the mechanics necessary for advanced applications.

An essential linear bipartite gate in the CV regime is realized by the quantum nondemolition (QND) coupling [25,26]. The QND feature of the gate guarantees many advantages in constructing quantum circuits [27–35]. This active transformation changes the total number of excitations in the coupled systems. In contrast to passive operations that do not influence the quantumness of the interacting parties (such as, e.g., a beamsplitter), a QND coupling can transform a classical input state into a nonclassical one. On the CV side, a pulsed QND interaction generates bipartite entanglement starting from the ground states of oscillators. This analysis and proposal have already been presented in Ref. [36].

At the same time, on the DV side, the active quadratic interactions can simultaneously produce pairs of different energy quanta in the subsystems beyond their classical states. This DV nonclassical coincidence analysis for the pulsed QND gate is still needed to complement the analysis of the Gaussian entanglement [36] and bunching of different quanta of energy [37]. It is relatively straightforward if the gate works as a two-mode hybrid amplifier, similar to the pioneering optical experiments [38]. In an ideal version of this case, the process produces quanta only in pairs, and their coincidence over the classical states of the subsystems is evaluated. This type of experiment has been carried out multiple times in optics

*Contact author: alisamanukhova@gmail.com; alisadmitrievna.manukhova@upol.cz
†Contact author: rakhubovsky@optics.upol.cz
‡Contact author: filip@optics.upol.cz

[39–41], atomic ensembles [42], and optomechanics [43]. However, the advantageous QND nature of the interaction complicates the evaluation, and another approach is needed with a detailed assessment of the hybrid protocol performance under realistic conditions.

In this paper, we propose a protocol and evaluation for a hybrid atom-mechanical QND gate to generate nonclassical coincidences of the quanta in a mechanical oscillator and an atomic ensemble. The hybrid pulsed gate was inspired by recent experimental advances [23,24] and evaluated in the context of the capability to create CV entanglement between atoms and mechanics as in Ref. [36]. In this paper, we show that this pulsed QND gate is capable of generating joint nonclassical single-quantum excitations in the hybrid system in the same relevant experimental regimes [23,24]. To prove our statement and quantify the result, we introduce thresholds for the probability of generating an excitation in both subsystems that are impossible to overcome with classical atom-mechanical states and show that the thresholds can be beaten by a feasible experiment. To understand it in detail, we investigate three different types of QND gates, i.e., atom-mechanical, atom-light, and optomechanical QND gates using feasible parameters and prove the possibility of generating nonclassical coincidences of excitations. We show that even for the noisy atom-mechanical and optomechanical QND gates, it is always possible to demonstrate the nonclassicality of the coincidences between quanta of different nature.

II. RESULTS

At the heart of our paper lies the scheme that allows establishing a nonlocal pulsed QND coupling between an ensemble of atoms and a mechanical oscillator, each in a separate cavity at a distance from each other. The scheme is inspired by recent experimental works [23,24] and was thoroughly investigated in the context of Gaussian CV entanglement generation [36]. To establish the gate, we couple the atomic cloud and mechanics using a pulse of squeezed light of duration τ with a rectangular temporal envelope that sequentially passes through atoms and mechanics accompanied by strong classical driving fields (see Fig. 1). The driving enables local QND interactions between the light and the corresponding matter mode in each of the cavities, and a proper feedforward operation allows establishing a QND gate between the atoms and the mechanics. In a strict sense, the cavities are not necessary for the implementation of the QND gate, however, their use enhances the coupling strength [44–47] and allows better control over the temporal mode-matching of the mediating pulse [48,49], increasing the overall efficiency. Furthermore, here we consider only the rectangular temporal shape of the pulse, which happens to closely approximate the optimal temporal mode of the pulse (the one maximizing the coupling and minimizing the noise contributions) and thus simplify the analytical expressions. A discussion of the implementation in more detail can be found in Ref. [36] and the Appendix.

In this section, we test a hybrid QND gate between an atomic ensemble and a mechanical oscillator to evaluate how much nonclassicality it brings into the initially classical state. We consider the normalized collective spins $(\hat{\mathbf{X}}_\mathrm{A}, \hat{\mathbf{P}}_\mathrm{A})$ as canonical atomic variables [50]. The mechanical part of the system is described by canonical quadratures $(\hat{\mathbf{X}}_\mathrm{M}, \hat{\mathbf{Y}}_\mathrm{M})$ that refer to the dimensionless position and momentum of the mechanical oscillator [51]. The quadratures of each of the modes are normalized such that $[\hat{\mathbf{X}}_k, \hat{\mathbf{P}}_k] = 2i$, with $k = \mathrm{A,M}$.

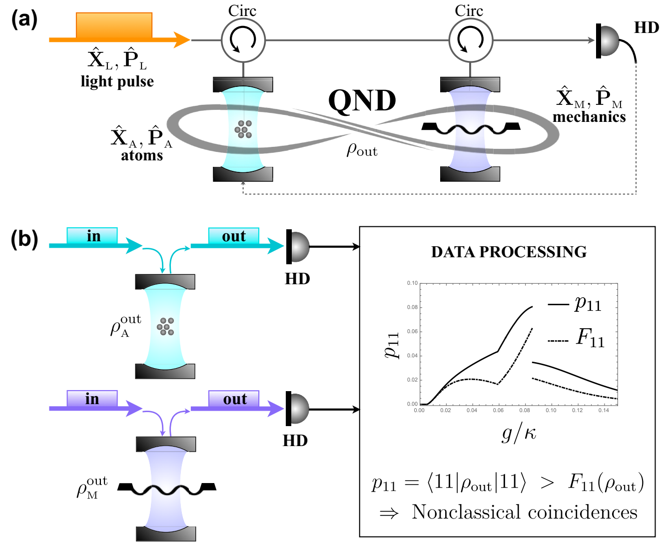

FIG. 1. (a) Scheme for the observation of nonclassical generation of boson pairs shared between atomic and mechanical oscillators. A QND gate between them, established using a mediating pulse and feedforward, generates quantum coincidences of matter excitations beyond the ones admitting a regular expansion over coherent states. HD: homodyne detector. Circ: circulator. (b) A potential scheme for verification of the nonclassical coincidences using light pulses for state transfer and homodyne detectors for the quantum states' estimation. Observation of coincidences p_{11} above the threshold F_{11} indicates that the output state of the atom-mechanical system is incompatible with the classical description.

The atom-mechanical QND gate transforms the vector of initial quadratures of the two-mode system $\mathbf{r}^{\mathrm{in}} = (\hat{\mathbf{X}}_\mathrm{A}^0, \hat{\mathbf{P}}_\mathrm{A}^0, \hat{\mathbf{X}}_\mathrm{M}^0, \hat{\mathbf{P}}_\mathrm{M}^0)^T$ to the vector of their final values $\mathbf{r} = (\mathbf{X}_\mathrm{A}, \mathbf{P}_\mathrm{A}, \mathbf{X}_\mathrm{M}, \mathbf{P}_\mathrm{M})^T$ as

$$\hat{\mathbf{X}}_\mathrm{A} = \hat{\mathbf{X}}_\mathrm{A}^0 - \mathfrak{G}\hat{\mathbf{X}}_\mathrm{M}^0 + \hat{\mathbf{N}}_{\mathrm{X}_\mathrm{A}}, \tag{1}$$

$$\hat{\mathbf{X}}_\mathrm{M} = \hat{\mathbf{X}}_\mathrm{M}^0 + \hat{\mathbf{N}}_{\mathrm{X}_\mathrm{M}}, \tag{2}$$

$$\hat{\mathbf{P}}_\mathrm{A} = \hat{\mathbf{P}}_\mathrm{A}^0 + \hat{\mathbf{N}}_{\mathrm{P}_\mathrm{A}}, \tag{3}$$

$$\hat{\mathbf{P}}_\mathrm{M} = \hat{\mathbf{P}}_\mathrm{M}^0 + \mathfrak{G}\hat{\mathbf{P}}_\mathrm{A}^0 + \hat{\mathbf{N}}_{\mathrm{P}_\mathrm{M}}. \tag{4}$$

For the derivation in full detail, we refer the reader to Ref. [36], while a summary is presented in the Appendix. The derivation is based on Heisenberg-Langevin equations, however, being open, the atom-mechanical system can benefit from tools of non-Hermitian physics [52,53]. From the input-output relations, it follows that the output quantum state of the system is fully determined by its initial state, the interaction gain $\mathfrak{G}$ tunable by manipulation with local interaction rates $g_{\mathrm{A,M}}$, and the only terms of the excess noise given by the operators $\hat{\mathbf{N}}_{\mathrm{X}_\mathrm{A},\mathrm{X}_\mathrm{M},\mathrm{P}_\mathrm{A},\mathrm{P}_\mathrm{M}}$. The additive noise inevitably arises due to the imperfections of the QND interaction. The imperfections include optical losses described by effective transmission η and interaction of the material modes with the environment, of which the most important is the mechanical heating, parametrized by the heating rate $\Gamma_M = \gamma_M n_{th}$ equal to the product of the mechanical viscous damping rate γ_M and the mean bath occupation n_{th}. Losses, including optical losses, spin decoherence, and mode mismatching, as well as thermal noise due to nonideal isolation of the mechanical mode from its thermal bath, both degrade the entangling process. However, their impact is not equivalent. Mechanical heating appears to be the most significant limiting factor that reduces the quality of the gate [36].

The protocol to establish the interaction is carried out in a way that ensures symmetry of the gate with equal interaction gain in Eqs. (1) and (4),

$$\mathfrak{G} = g_M g_A \frac{2\tau\sqrt{\eta}}{\kappa}\left[1 + e^{-\kappa\tau} - \frac{2}{\kappa\tau}(1 - e^{-\kappa\tau})\right], \tag{5}$$

where $g_{A,M}$ are the interaction rates of the local intracavity QND interactions and κ is the cavity linewidth. For simplicity, we assume equal linewidths κ and equal gains g for both the light-atom and optomechanical interactions. This is feasible experimentally [23,24], provides nearly optimal temporal mode-matching (and hence stronger atom-mechanical coupling), and allows simplifying the analytical treatment.

In the case of negligible noise, this transformation corresponds to a unitary QND interaction between the mechanical and atomic systems with the evolution operator:

$$\hat{\mathcal{U}} = \exp[-i\mathfrak{G}\hat{\mathbf{X}}_M\hat{\mathbf{P}}_A/2]. \tag{6}$$

Starting with the Gaussian product state, the system is driven towards another Gaussian state that might exhibit nonclassicality in the form of coincidences of excitations.

To study the capability of such a gate to generate nonclassical coincidence between energy quanta in the atoms and mechanics, let us first introduce a suitable witness of nonclassicality. We are motivated by the optical experiments [39–41], however, we adopt feasible homodyne detection similarly to how it was already recently used in Ref. [54]. It is suitable for the detection of both atomic and mechanical subsystems [50,55,56]. From a direct measurement of the covariance matrix, we can calculate elements of the density matrix in the Fock-states basis and obtain adequate predictions in the Gaussian approximation.

Here, we use the definition that a state ρ_c of a linear harmonic oscillator is classical whenever its expansion in the coherent state basis yields a P function that is a regular probability density function [57,58], and nonclassical otherwise. This definition of nonclassicality led to the development of a plethora of experimentally applicable criteria (for example, see Refs. [59,60] and references therein). More challenging witnesses of nonclassicality such as negativity of the Wigner function (WF) [61] provide *sufficient* criteria of nonclassicality, but not the *necessary* criteria.

To assess the coincidence of different energy quanta at the output of the gate, we evaluate the matrix element $p_{11}(\rho_{out}) \equiv \langle 11|\rho_{out}|11\rangle$, which is the probability of detecting exactly one excitation at each output, in the atomic ensemble and the mechanical oscillator, and compare it with the corresponding nonclassicality threshold $F_{11}(\rho_{out})$. The threshold is *state dependent* and is defined as the maximal value of the probability p_{11} achievable with classical states that have the same vacuum contributions in the individual subsystems as state ρ_{out}:

$$F_{11}(\rho) \equiv \max_{\rho_c} p_{11}(\rho_c),\ \text{over classical } \rho_c \text{ such that}$$
$$p_{0A}(\rho_c) = p_{0A}(\rho) \text{ and } p_{0M}(\rho_c) = p_{0M}(\rho), \tag{7}$$

where we define the vacuum contribution of the first (atomic) mode as $p_{0A}(\rho) = \mathrm{Tr}_M\langle 0_A|\rho|0_A\rangle$ and, similarly, mechanical $p_{0M}(\rho) = \mathrm{Tr}_A\langle 0_M|\rho|0_M\rangle$. Whenever a state ρ_{out} has $p_{11}(\rho_{out}) > F_{11}(\rho_{out})$, this state is nonclassical, as the threshold F_{11} includes optimization over all suitable classical states. The resulting nonclassicality, therefore, originates from an active quadratic operation embodied by the atom-mechanical QND gate.

The threshold F_{11} can be computed as follows. For a given output bipartite state ρ_{out} we first compute the vacuum contributions $p_{0A}(\rho_{out})$ of the atomic mode and $p_{0M}(\rho_{out})$. A coherent state $|\alpha\rangle$ with vacuum contribution $p_0 = |\langle\alpha|0\rangle|^2$ has the single-photon probability given by

$$|\langle\alpha|1\rangle|^2 = p_1^c(p_0) \equiv -p_0 \ln p_0. \tag{8}$$

The product

$$F_{11}(\rho_{out}) \equiv p_1^c(p_{0A}(\rho_{out})) \times p_1^c(p_{0M}(\rho_{out})) \tag{9}$$

is then the maximal probability p_{11} attainable by *pure* coherent states with exactly same vacuum contributions as state ρ_{out}. The proof that $F_{11}(\rho_{out})$ is, in fact, the maximal probability p_{11} reachable with arbitrary classical states (constrained by vacuum probabilities matching the ones of ρ_{out}) is in the Appendix.

As a paradigmatic example, we consider coherent states at each of the inputs: $\rho^{in} = \rho^{coh} = |\alpha_a\rangle\langle\alpha_a| \otimes |\beta_b\rangle\langle\beta_b|$. We study the evolution of such a state passing the gate and evaluate the p_{11} contribution in the output state, comparing it with the nonclassicality threshold F_{11}. The input state ρ^{coh} is fully characterized by the vector of the mean values of the quadratures $\mathbf{R} = \langle (X_a, Y_a, X_b, Y_b)^T\rangle$. We optimize over the elements of this vector to achieve the strongest advantage of the corresponding output p_{11} contribution over the threshold F_{11}. Formally, the quantity being maximized is the nonclassicality witness:

$$\Delta \equiv \max\left[0, \langle 11|\rho_{out}^{coh}|11\rangle - F_{11}\left(\rho_{out}^{coh}\right)\right]. \tag{10}$$

In general, Δ is a function of the input state (which is equivalent to being a function of $\mathbf{R}$) and the physical parameters of the gate (which include local coupling rates $g_{A,M}$, duration of the mediating pulse τ, etc.). For each set of the physical parameters, the nonclassicality witness Δ is optimized over the four elements of $\mathbf{R}$ that fully determine the input state. The optimization is necessary since not for every $\mathbf{R}$ the output state surpasses the threshold F_{11}. Fortunately, in a wide range of gate configurations, the optimization returns the vacuum input as the optimal one. Nevertheless, as shown below, for any particular set of the physical parameters of the gate, it is possible to specify an initial $\mathbf{R}$ allowing us to reach or overcome the nonclassicality threshold.

Figure 2 demonstrates the results of maximization of the nonclassicality witness for the atom-mechanical QND gate with feasible physical parameters which are either taken from Refs. [23,24] or are within reach of those experiments (see Appendix for a discussion of feasibility). The maximization

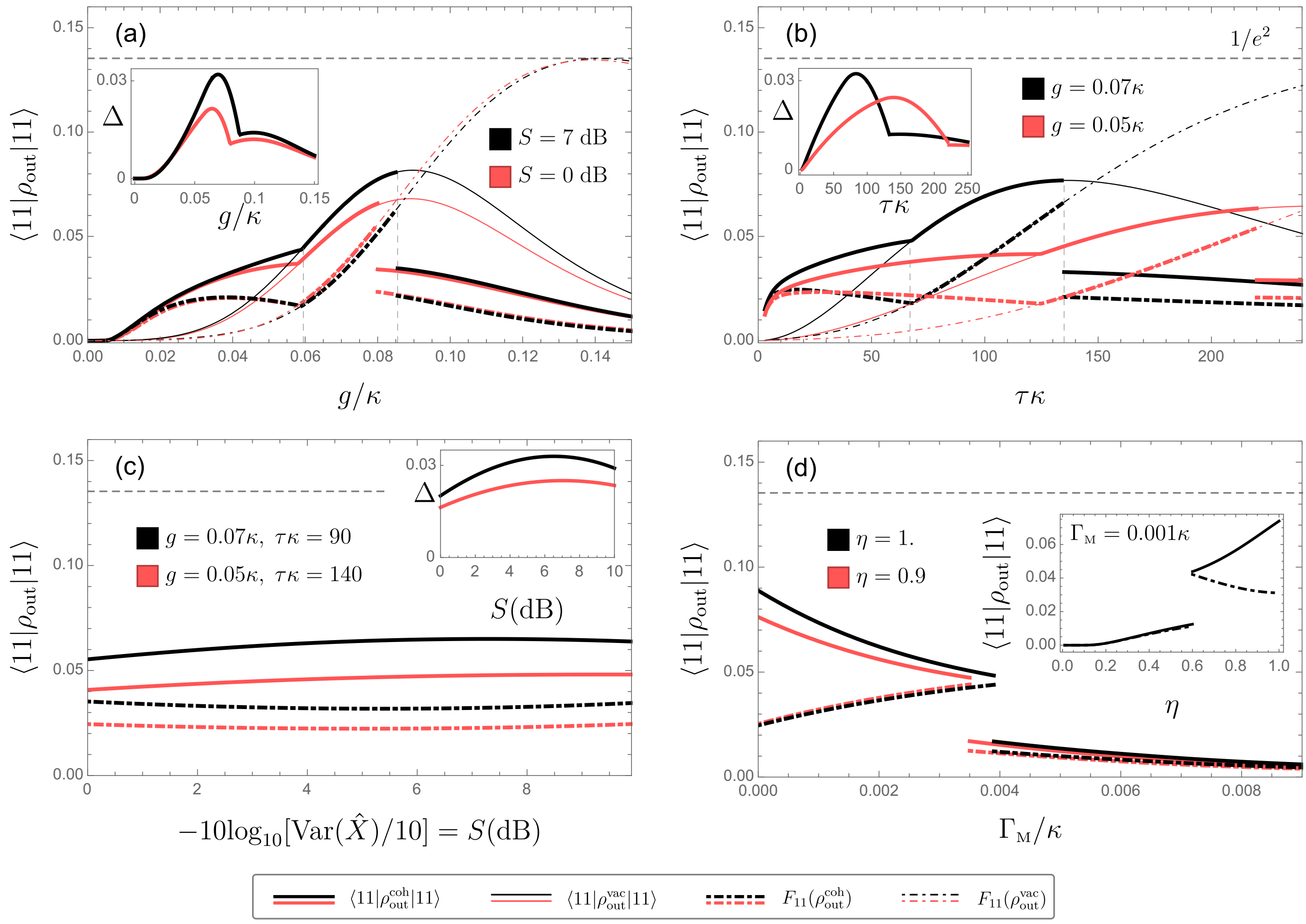

FIG. 2. Nonclassical coincidence probability $\langle 11|\rho_{out}|11\rangle$ at the output of the atom-mechanical QND gate given coherent states at the input. Matrix elements $\langle 11|\rho_{out}|11\rangle$ (solid curves) and nonclassicality thresholds $F_{11}(\rho_{out})$ (dot-dashed curves) for state ρ_{out} at the output of atom-mechanical QND gate with coherent states at the input. Thick curves are calculated using the vector of means of ρ^{coh} providing the maximal advantage Δ [defined in Eq. (10)]. Thin curves correspond to the matrix elements of the output state of the gate with the vacuum input. (a) Dependence on the coupling strength for different squeezing (black for 7 dB, red for 0 dB), assuming $g = g_A = g_M$; (b) dependence on the pulse duration τ for different coupling strengths (black for $g = 0.07\kappa$, red for $g = 0.05\kappa$). In (a) and (b), thin vertical lines indicate the value of the arguments at which the optimal family of the input state changes. (c) Dependence on the squeezing (black for $g = 0.05\kappa,\ \tau\kappa = 140$, red for $g = 0.07\kappa,\ \tau\kappa = 90$). (d) Dependence on the rethermalization rate for different efficiencies for $g = 0.07\kappa$. The inset shows dependence on the efficiency. Even for low efficiency and high rethermalization it is possible to find an input state providing positive advantage Δ. Numerical parameters, where not specified otherwise, are $\tau = 90/\kappa$, $\eta = 0.9$, $\Gamma_M = 10^{-3}\kappa$, $S = 7$ dB.

assumes equal local coupling rates $g = g_A = g_M$, the regime achieved in hybrid systems [23,24], and reachable by a number of optomechanical and atomic setups [62–64]. The matrix element $\langle 11|\rho_{out}|11\rangle$ (solid curves) is compared with the corresponding nonclassicality threshold (dot-dashed curves). The curves have a noticeable discontinuity which is explained by the design of the figure of merit. At each point along the x axis, the solid and dashed lines show the quantities corresponding to the value of $\mathbf{R}$ that maximizes *the difference* between these curves. Although the difference itself changes continuously along the x axis, the corresponding element and threshold are not necessarily continuous which is the case in Figs. 2(a), 2(b) and 2(d) (see Appendix for further discussion).

Figures 2(a) and 2(b) show dependencies of p_{11} and F_{11} on the coupling strength g and the mediating pulse duration τ for the other fixed parameters. An increase in both g and τ increases the overall gain $\mathfrak{G}$ of the gate, and therefore the traces in the panels exhibit similar behavior. The other parameters of the gate, such as added noise, change differently and hence the panels are not fully equivalent. All the dependencies show rather similar behavior and consist of a few regions. The region corresponding to lower gain shows increasing probability p_{11} and the advantage Δ with increasing gain $\mathfrak{G}$. The optimal input state is described by nonzero elements of $\mathbf{R}$ that decrease as the gain increases. Importantly, the figure of merit that we use is phase insensitive and does not change upon rotation of the output state in the phase space. This phase insensitivity thus ensures that there are multiple optimal input states for each value of the gain. Eventually, at a certain value of the gain, the second region, delivered from input vacuum ($\mathbf{R} = \mathbf{0}$) takes over (thin lines show the functions corresponding to the vacuum input also for the values of the gain where input vacuum is not optimal). Importantly, this region spans over a significant volume in the parameter space. The optimal nonclassicality witness can thus be observed in this region without the need to optimize the input states carefully. Finally, at the stronger gains, the third region starts giving the optimal advantage Δ. Along this region, the optimal initial state is described again by nonzero displacements that grow with further increase of the gain. (See the Appendix for further discussion.)

There are important differences between Figs. 2(a) and 2(b). Dependence on g demonstrates Δ close to zero for small values of g. However, this is not observed for the dependence on τ. This is due to the presence of noise in the system, which, due to the peculiarity of the QND gate (specifically chosen feed-forward procedure), cannot be fully compensated (even by setting the unrealistic condition of zero optical loss and zero rethermalization). Thus, if the coupling strength g is near zero (here, $g \lesssim 0.02\kappa$, however, in general, the approximate boundary coupling value is set by the other gate parameters), it is impossible for $\langle 11|\rho_{\text{out}}|11\rangle$ to surpass the threshold. For Fig. 2(b) showing the dependence on τ, the coupling strength is already chosen to be sufficient, so $\Delta > 0$ for any $\tau > 0$.

Figure 2(c) shows the dependence of the element p_{11} on squeezing of the mediating optical pulse. There exists an optimal value of squeezing around moderate $S = 7$ dB. Importantly, despite the existence of the maximum, the overall dependence is rather weak, such that a reasonable advantage can be achieved by the gate even in the absence of the squeezing. Figure 2(d) demonstrates the limits of the robustness of the nonclassicality witness with respect to imperfections. In the main plot, the p_{11} is shown as a function of the mechanical heating rate Γ_{M} that appears to be the main limiting factor in the scheme. As expected, with an increase of Γ_{M} the nonclassicality decreases and eventually vanishes. In the inset, the element is evaluated as a function of the effective transmittance of the optical loss in the mediating channel (in the lossless case, $\eta = 1$). As the loss increases, the advantage vanishes if around 40% photons are lost.

III. NONCLASSICAL COINCIDENCES IN ATOM-LIGHT AND OPTOMECHANICAL SYSTEMS

To understand the overall performance of the parts, we separately examine the atom-light QND gate, the first of the two local QND gates that allow establishing the nonlocal atom-mechanical gate. The gate couples a quantum state of a certain temporal mode of a propagating light pulse to the collective excitations of an ensemble of atoms in a cavity [36,50]. As previously, we assume a coherent input state in both atomic ensemble and light and analyze the possible probability to have a single excitation in each output.

The atom-light interaction inside the cavity is due to Faraday rotation and is described by an effective QND-type Hamiltonian $\hat{H}_{\text{LA}} = \hbar g_{\text{A}} \hat{\mathbf{X}}_{\text{A}} \hat{p}_{\text{c}}$, where g_{A} is the coupling rate and $\hat{p}_{\text{c}}$ is the canonical phase quadrature of the intracavity light. Then the signal leaves the atomic cavity and at the output can be derived using the input-output relations. At this stage, we also take into account the loss that occurs during the coupling process.

The bipartite atom-light system is described by a vector of canonical quadrature operators $(\hat{\mathbf{X}}_{\text{A}}, \hat{\mathbf{P}}_{\text{A}}, \hat{\mathbf{X}}_{\text{L}}, \hat{\mathbf{P}}_{\text{L}})^T$ where the former two correspond to collective spin excitations, and the latter two to a certain temporal mode of light. The interaction maps the initial values $\hat{\mathbf{Q}}_i^0$ of these operators onto the final values $\hat{\mathbf{Q}}_i$ in the following way:

$$\hat{\mathbf{X}}_{\text{A}} = \hat{\mathbf{X}}_{\text{A}}^0 + \hat{\mathbf{N}}_{\text{X}_{\text{A}}}, \tag{11}$$

$$\hat{\mathbf{X}}_{\text{L}} = \hat{\mathbf{X}}_{\text{L}}^0 + \mathsf{G}_{\text{L}} \hat{\mathbf{X}}_{\text{A}}^0 + \hat{\mathbf{N}}_{\text{X}_{\text{L}}}, \tag{12}$$

$$\hat{\mathbf{P}}_{\text{A}} = \hat{\mathbf{P}}_{\text{A}}^0 - \mathsf{G}_{\text{A}} \hat{\mathbf{P}}_{\text{L}}^0 + \hat{\mathbf{N}}_{\text{P}_{\text{A}}}, \tag{13}$$

$$\hat{\mathbf{P}}_{\text{L}} = \hat{\mathbf{P}}_{\text{L}}^0 + \hat{\mathbf{N}}_{\text{P}_{\text{L}}}. \tag{14}$$

Same as previously, the excess noise terms $\hat{\mathbf{N}}_{\text{X}_{\text{A}},\text{X}_{\text{L}},\text{P}_{\text{A}},\text{P}_{\text{L}}}$ are characterized by the physical parameters of the system. In the case of state-of-the-art experiments with atomic ensembles [55], these noise terms are dominantly vacuum.

Unlike the atom-mechanical QND gate, the atom-light gate is asymmetric, which formally manifests in the interaction gains being unequal ($\mathsf{G}_{\text{A}} \neq \mathsf{G}_{\text{L}}$): This asymmetry is caused by the cavity memory effect and the optical losses,

$$\mathsf{G}_{\text{A}} = g_{\text{A}} \sqrt{\frac{2\tau}{\kappa_{\text{A}}}}, \tag{15}$$

$$\mathsf{G}_{\text{L}} = g_{\text{A}} \sqrt{\frac{2\tau}{\kappa_{\text{A}}}} \times \sqrt{\eta} \left[1 - \frac{1 - e^{-\kappa_{\text{A}}\tau}}{\kappa_{\text{A}}\tau} \right], \tag{16}$$

where κ_{A} is the linewidth of the cavity containing the atomic ensemble and τ is the optical pulse length.

Let us test how much nonclassicality can introduce the asymmetric atom-light gate to a classical state used as an initial state.

Figure 3(a) shows the matrix element $p_{11} = \langle 11|\rho_{\text{out}}|11\rangle$ (with solid lines) compared with the corresponding nonclassicality threshold F_{11} (dot-dashed curves). Along the x axis, both subsystems are assumed to be prepared in coherent states, such that they maximize the advantage of the element p_{11} over the corresponding threshold F_{11}. The matrix elements are shown as functions of the coupling strength g_{A} for the fixed pulse duration τ. In this case, an increase of g is approximately equivalent to an increase of the gains $\mathsf{G}_{\text{A,L}}$. Qualitatively, the performance of the atom-light gate is very similar to the atom-mechanical case. The main limiting factor for this system appears to be the optical efficiency, that is, photon loss. For the small optical losses, the best advantage is achieved using the vacuum input. With an increase of the losses, the probability p_{11} decreases, but it is always possible to optimize the input states so at the output a nonclassicality witness Δ is positive.

Moreover, for small optical losses, the value of p_{11} can exceed $1/e^2$, the maximal p_{11} attainable with *arbitrary* classical states. The atom-light gate is thus capable of surpassing an even more stringent nonclassicality threshold than F_{11}. At the same time, the asymmetry of the coupling gains does not impede the output probability p_{11} to surpass the threshold F_{11}.

In the second part, we examine optomechanical QND interaction that can be realized by modulating the optomechanical coupling rate at twice the frequency of the mechanical

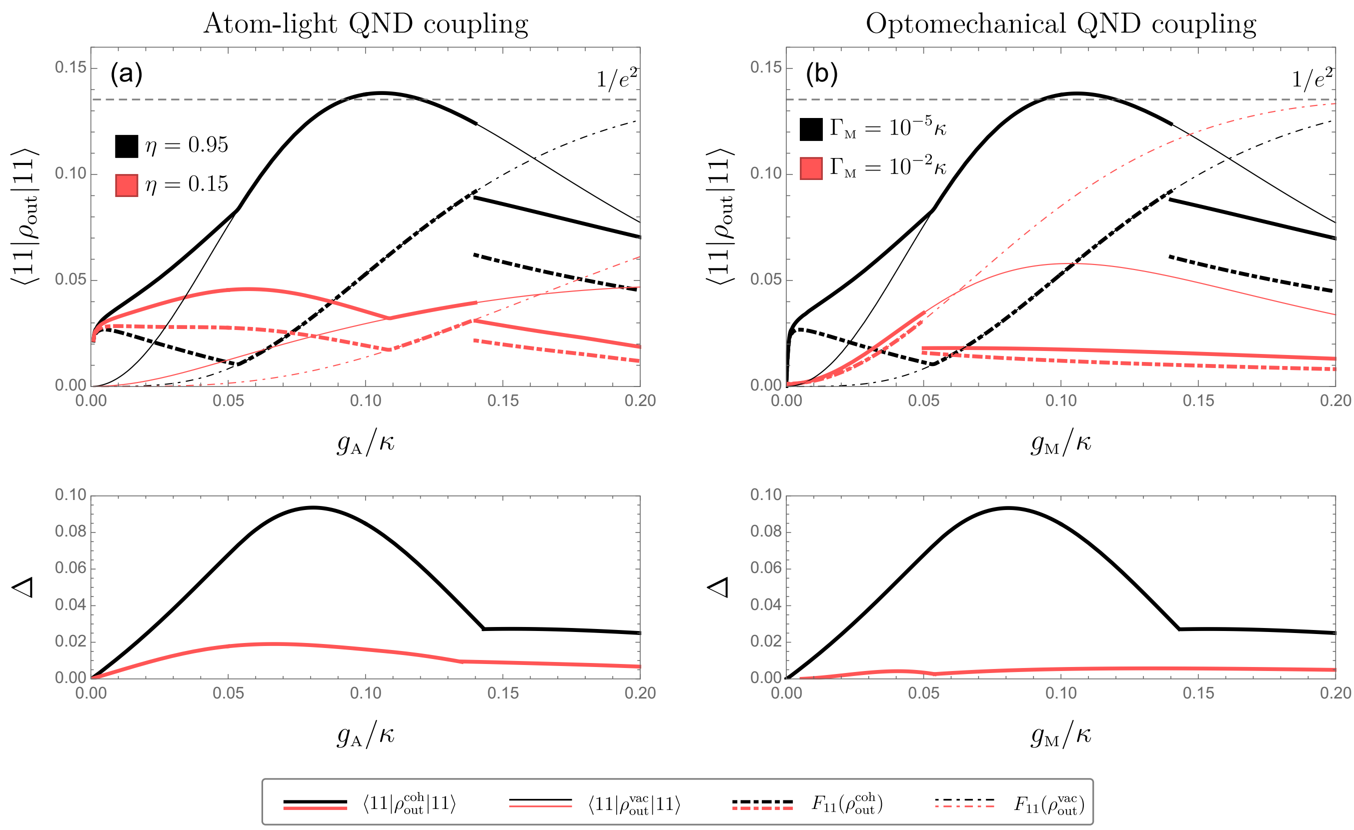

FIG. 3. Nonclassical coincidence probability $\langle 11|\rho_{out}|11\rangle$ at the output of a QND interaction in (a) atom-light system (b) optomechanical system. Matrix elements $\langle 11|\rho_{out}|11\rangle$ at the output (solid curves) and corresponding nonclassicality thresholds $F_{11}(\rho_{out})$ (dot-dashed curves) given coherent states at the input. Thick curves correspond to the input state that provides maximal advantage Δ [defined in Eq. (10)] at the output. Thin curves correspond to vacuum input. The dashed gray line is the output classical threshold ($1/e^2$). The numerical parameters are (a) pulse duration $\tau = 90/\kappa$, efficiencies $\eta = 0.95$ for black and $\eta = 0.15$ for red, (b) $\tau = 90/\kappa$, $\eta = 0.95$, and rethermalization rates $\Gamma_M = 10^{-5}\kappa$ for black and $\Gamma_M = 10^{-2}\kappa$ for red.

oscillator [52]. This scheme was proposed by Braginsky [25] to achieve back-action evasion for mechanical displacement detection and has been implemented in electromechanics [65,66] and optomechanics [67,68].

Despite the different nature of the QND interaction, the mathematical description of the atom-light and optomechanical gates is in the end the same. The input-output relations for the optomechanical gate can be obtained from Eqs. (11) to (14) by replacing $A \rightarrow M$. The same replacement allows us to obtain the gains $G_{L,M}$ from Eqs. (15) and (16). A critical difference to the atom-light interaction stems from the mechanical oscillator being coupled to a hot thermal environment. This gives rise to rethermalization at rate Γ_M which significantly contributes to the added noise $\mathbf{N}$.

The role of thermal noise is investigated in Fig. 3(b), where we plot the contribution p_{11} and the corresponding threshold F_{11} for the output states. As previously, the plots are produced assuming coherent states at the input, with optimization over these input states such that delivers maximal advantage Δ [defined in Eq. (10)]. The presence of the thermal noise significantly decreases both the output contribution p_{11} and the advantage Δ. A decrease of the rethermalization rate allows us to approach the regime of nearly unitary interaction. Indeed, if the rethermalization rate is low enough ($\Gamma_M \approx 10^{-5}\kappa$ is sufficient), the difference between the atom-light and optomechanical cases vanishes. Finally, for the small optical losses and low enough rethermalization, the value of $\langle 11|\rho_{out}|11\rangle$ surpasses the stringent threshold $1/e^2$.

IV. DISCUSSION AND OUTLOOK

To summarize, in this paper, we consider the capability of a realistic pulsed QND gate to create nonclassical coincidences of excitations in the coupled subsystems. We do this for the local pulsed atom-light and optomechanical gates, induced by interaction with a pulse of squeezed light. We test the nonclassicality of the nonlocal atom-mechanical gate resulting from the sequential application of the two local ones as well. Each of these gates can demonstrate nonclassicality of quanta coincidences in the form of positive witness Δ [defined in Eq. (10)], moreover, the local atom-light and optomechanical gates are capable of overcoming a more stringent threshold $p_{11} > 1/e^2$. To reach a nonclassical regime, an optimization of the input coherent states of atoms and mechanics could be useful. Importantly, the p_{11} contribution of the output state only weakly depends on the mediating pulse squeezing. This allows the implementation of our proposed scheme using coherent light passing through atomic and mechanical subsystems instead of squeezed light.

An experimental test of the scheme we investigated would cover the previously unexplored discrete-variable properties of a basic quantum nondemolition Gaussian interaction, important for the quantum circuits with continuous variables [27–35]. At the practical level, it can help development of hybrid platforms comprising disparate subsystems thus capable of overcoming drawbacks of the constituents [1–3,69]. Simultaneously, such a test would cover an additional facet of the interaction in the hybrid atom-mechanical system that is a prospective candidate for quantum metrology [70–72].

The verification of nonclassical coincidences is a crucial initial milestone for further developments, as has been demonstrated, for example, for optomechanical systems [43]. Following this essential step for hybrid coincidences, the next milestones for continuous-variable development include the heralded nonclassical and quantum non-Gaussian states [73,74], later eventually with negative Wigner functions [75,76]. For discrete-variable approaches, the nonclassical coincidences can be extended to entanglement between two quanta in different modes of atoms and mechanics, similar to what has already been achieved in atomic-atomic [73,77] and mechanical-mechanical systems [78,79].

Our general approach allows generalizing the conclusions to other hybrid systems capable of reaching local QND interactions [8]. Besides this, nonclassical correlations between atoms and mechanics can possibly allow conditional control using measurement-based techniques, demonstrated previously with atoms [77,80] and mechanics [81–83]. Furthermore, implementation of single-excitation detection opens the way to quantum non-Gaussian states preparation in material systems [84,85]. Quantum non-Gaussian states hold the potential to provide an advantage in metrology and sensing [86,87] as it was shown with ions [88]. An interface to the mechanical systems with nonlinear motional potentials [10,89] can, in principle, allow one to translate the nonlinearity to the dynamics of the atomic excitations. Optical coupling of the subsystems is capable of interfacing very disparate distant components, which permits thinking of assembling arrays of such atom-mechanical systems. Combined with operations at a single-excitation level this perspective opens a way to topological atom-optomechanics [90].

The data sets generated and analyzed during the current paper are available from the corresponding author on reasonable request .

ACKNOWLEDGMENTS

The authors acknowledge Project No. 23-06308S of the Czech Science Foundation and Project No. CZ.02.01.01/00/22_008/0004649 of the Czech Ministry of Education, Youth and Sport (MEYS). A.D.M and R.F. also acknowledge the support of national funding from MEYS and the European Union's Horizon 2020 (20142020) research and innovation framework program under the grant agreement program under Grant No. 731473 (Project No. 8C20002 ShoQC). Project ShoQC has received funding from the QuantERA ERA-NET Cofund in Quantum Technologies implemented within the European Union's Horizon 2020 program.

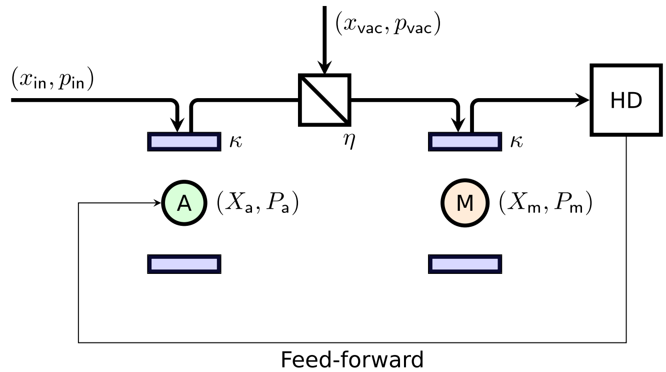

FIG. 4. Sketch of the proposed setup to realize the QND gate between atoms (A) and mechanics (M). HD:- Homodyne detector.

R.F. developed the theoretical idea and supervised the project. A.D.M. performed calculations and made the figures with input from A.A.R. All authors jointly contributed to the analysis and preparation of the paper.

The authors declare no competing interests.

APPENDIX

1. Pulsed atom-mechanical qnd gate

To make the present paper self-consistent, in this section, we recapitulate the relevant findings of Ref. [36] regarding the proposed atom-mechanical QND gate. In particular, we sketch the steps required to write the equations of motion for the system quadratures and to arrive at the input-output transformations for the quadratures of the atomic and mechanical systems. For a full derivation with more detail, we address the reader to Ref. [36].

The atom-mechanical gate is based on two cavities with equal linewidths κ, the first containing an atomic ensemble, and the second a mechanical oscillator (see Fig. 4). A pulse of quantum squeezed light with a rectangular temporal profile sequentially passes the atomic ensemble in a cavity and then the optomechanical cavity. Subsequently, the pulse is detected via a homodyne measurement. The classical optical drives, shone upon the cavities together with the quantum light, enable local QND coupling of the matter modes (atoms or mechanics) with the intracavity light during the intervals of the mediating pulse passing the corresponding cavity. Importantly, by choosing the drive phases, these QND interactions couple to the orthogonal quadratures of the mediating pulse (see formal details below). A quadrature of the mediating pulse leaking from the mechanical cavity is detected by a quadrature measurement (homodyne). The result of the homodyne detection is used to displace (via a classical feed-forward) the atomic ensemble in the phase space.

To describe the dynamics of the system, we use Heisenberg-Langevin equations for the phase-space quadratures of the participating subsystems. Given that the Hamiltonians of each interaction are at most quadratic in the variables, all the initial quantum states and the quantum states of all the inputs are Gaussian, the system can be fully described by input-output relations for the quadratures.

The matter systems are described by the (dimensionless) canonical quadratures $(X_{\mathrm{a}}, P_{\mathrm{a}})$ for atoms and $(X_{\mathrm{m}}, P_{\mathrm{m}})$ for the mechanical oscillator. Here and below, all the canonical quadratures are normalized such that $[X_i, P_i] = 2\mathrm{i}$ if not specified otherwise. These modes are initialized in coherent states (formal definitions below).

The mechanical oscillator is coupled at rate γ_{M} to the bath described by the quadratures $(\zeta_{\mathrm{X_m}}(t), \zeta_{\mathrm{P_m}}(t))$: $[\zeta_{X_{\mathrm{m}}}(t), \zeta_{P_{\mathrm{m}}}(t')] = 2\mathrm{i}\delta(t-t')$. These quadratures describe a thermal state with mean occupation n_{th}: $\langle \frac{1}{2}(\zeta_i(t)\zeta_i(t') + \zeta_i(t')\zeta_i(t))\rangle = (2n_{\mathrm{th}}+1)\delta(t-t')$, where $i = X_{\mathrm{m}}$ or P_{m}. The quantity n_{th} is defined by the Bose-Einstein statistics: $n_{\mathrm{th}} = k_{\mathrm{B}}T/\hbar\Omega_{\mathrm{m}}$, where k_{B} is Boltzmann's constant, T is the effective temperature of the mechanical environment, and Ω_{m} is the frequency of the mechanical oscillator. Together, γ_{M} and n_{th} form the *reheating rate* $\Gamma_{\mathrm{M}} = \gamma_{\mathrm{M}}(n_{\mathrm{th}} + 1/2) \approx \gamma_{\mathrm{M}} n_{\mathrm{th}}$.

The coupling of the atomic oscillator to its vacuum environment is negligible during the gate operation.

Prior to impinging on the atomic cavity, the mediating pulse is described by the quadratures $(\hat{x}_{\mathrm{in}}(t), \hat{p}_{\mathrm{in}}(t))$, such that $[\hat{x}_{\mathrm{in}}(t), \hat{p}_{\mathrm{in}}(t')] = 2\mathrm{i}\delta(t-t')$. Other parameters: pulse duration τ, squeezing value S.

The intracavity fields are described by canonical variables $(\hat{\mathbf{X}}_0, \hat{\mathbf{P}}_0)$ and $(\hat{\mathbf{X}}'_0, \hat{\mathbf{P}}'_0)$. Initially, these fields are in a vacuum.

Within the cavities, the optical pulse is coupled to atoms and mechanics, respectively, via QND interactions enabled by strong classical optical pumps. The Hamiltonians of the atom-light interaction (H_{AL}) and the optomechanical interaction (H_{OM}) read, correspondingly,

$$H_{\mathrm{AL}} = g_{\mathrm{a}} P_{\mathrm{a}} \hat{\mathbf{X}}_0, \quad H_{\mathrm{OM}} = g_{\mathrm{m}} X_{\mathrm{m}} \hat{\mathbf{P}}'_0, \tag{A1}$$

where $g_{\mathrm{a,m}}$ are the coupling rates.

We also use the input-output relations for the light which, for brevity, we write for annihilation operators a. For a mode with quadratures x, p, the annihilation operator reads $a = (x + \mathrm{i}p)/2$, and the input-output relations are as follows:

$$a^{(i)}_{\mathrm{out}} = -a^{(i)}_{\mathrm{in}} + \sqrt{2\kappa}\, a^{(i)}_{\mathrm{intracav}}, \tag{A2}$$

where i labels different cavities,

The Hamiltonians (A1) with the input-output relations are used to write the Heisenberg-Langevin equations. The input light of the mechanical cavity is obtained as the attenuated output light of the cavity containing atoms with an admixture of vacuum (again, for annihilation operators for brevity):

$$a^{(\mathrm{M})}_{\mathrm{in}} = \sqrt{\eta}\, a^{(\mathrm{A})}_{\mathrm{out}} + \sqrt{1-\eta}\, a^{(\mathrm{vac})}. \tag{A3}$$

The homodyne detection of the light quadrature X data is used to control the feed-forward procedure to shift the atomic quadratures. The homodyne output is the quantity

$$P_{\mathrm{HD}} = \frac{1}{\sqrt{\tau}} \int_0^{\tau} \mathrm{d}s\, P^{(\mathrm{M})}_{\mathrm{out}}(s), \tag{A4}$$

used to displace the atomic oscillator,

$$\hat{P}_{\mathrm{a}} \mapsto \hat{P}_{\mathrm{a}} + K P_{\mathrm{HD}}, \tag{A5}$$

where K is the feed-forward gain.

Note that here we consider homodyne detection of a flat-top temporal mode of the leaking light for the following reasons. Driving of the optomechanical cavity with a constant power for a duration $0 \leqslant t \leqslant \tau$ generates a QND interaction (A1) of approximately constant strength g_{m} (up to the transient effects relevant at timescales $\kappa t \sim 1$). As a consequence of this coupling, the leaking light's amplitude quadrature picks up information about the mechanical position quadrature in the form

$$\begin{aligned} P^{(\mathrm{M})}_{\mathrm{out}}(t) &= \cdots + X_{\mathrm{m}}(0)\sqrt{\frac{2}{\kappa}}\, g_{\mathrm{m}}(1 - \mathrm{e}^{-\kappa t}) \\ &\underset{\kappa\tau \gg 1}{\approx} \cdots + X_{\mathrm{m}}(0)\sqrt{\frac{2}{\kappa}}\, g_{\mathrm{m}}. \end{aligned} \tag{A6}$$

This equation indicates that for long pulses, $\kappa\tau \gg 1$, the rectangular temporal profile closely approximates the optimal pulse profile that maximizes the contribution of $X_{\mathrm{m}}(0)$ in the homodyne output.

After the pulsed interactions, homodyne detection, and feedforward are done, the quadratures of the atoms and the mechanical oscillator read

$$\hat{X}_{\mathrm{a}} = \hat{X}^{\mathrm{in}}_{\mathrm{a}} + \hat{N}_{X_{\mathrm{a}}}, \tag{A7}$$

$$\hat{P}_{\mathrm{a}} = \hat{P}^{\mathrm{in}}_{\mathrm{a}} + \mathsf{G}\hat{P}^{\mathrm{in}}_{\mathrm{m}} + \hat{N}_{P_{\mathrm{a}}}, \tag{A8}$$

$$\hat{X}_{\mathrm{m}} = \hat{X}^{\mathrm{in}}_{\mathrm{m}} - \mathsf{G}\hat{X}^{\mathrm{in}}_{\mathrm{a}} + \hat{N}_{X_{\mathrm{m}}} \tag{A9}$$

$$\hat{P}_{\mathrm{m}} = \hat{P}^{\mathrm{in}}_{\mathrm{m}} + \hat{N}_{P_{\mathrm{m}}}, \tag{A10}$$

with G being the effective gate gain, defined as

$$\mathsf{G} = g_{\mathrm{a}} g_{\mathrm{m}} \sqrt{\eta}\, \frac{2}{\kappa^2}(e^{-\kappa t}(\kappa\tau + 2) + \kappa\tau - 2), \tag{A11}$$

and $\hat{N}_{X_{\mathrm{a}}, P_{\mathrm{a}}, X_{\mathrm{m}}, P_{\mathrm{m}}}$ denoting the noise contributions. These noise terms originate from the optical vacuum noise, mechanical thermal noise, and the initial intracavity vacuum. The explicit expressions for them are rather involved:

$$\hat{N}_{X_{\mathrm{a}}} = 0, \tag{A12}$$

$$\hat{N}_{P_{\mathrm{a}}} = B\, \hat{\mathbf{X}}^{\mathrm{in}} + C\, \hat{\mathbf{X}}^{\mathrm{in}}_f + D\, \hat{\mathbf{X}}^{\mathrm{vac}} + F\, \hat{\boldsymbol{\zeta}}^{P_{\mathrm{m}}}_f + H\, \hat{\mathbf{X}}_0 + J\, \hat{\mathbf{X}}'_0 \tag{A13}$$

$$\hat{N}_{X_{\mathrm{m}}} = L\, \hat{\mathbf{P}}'_0 + A\, \hat{\boldsymbol{\zeta}}^{X_{\mathrm{m}}} + M\, \hat{\mathbf{P}}^{\mathrm{in}} + R\, \hat{\mathbf{P}}_0 + U\, \hat{\mathbf{P}}^{\mathrm{vac}}, \tag{A14}$$

$$\hat{N}_{P_{\mathrm{m}}} = A\, \hat{\boldsymbol{\zeta}}^{P_{\mathrm{m}}}, \tag{A15}$$

where we used the following dimensionless coefficients:

$$\begin{aligned} &A = \sqrt{\tau 2\Gamma_m}, \quad B = -\frac{g_{\mathrm{a}}\sqrt{2}}{\mathbf{K}_2\sqrt{\kappa}}, \quad C = \frac{\mathbf{K}_f}{\mathbf{K}_5}\sqrt{\frac{\eta}{\tau}}, \\ &D = \frac{\mathbf{K}_f}{\mathbf{K}_1}\sqrt{\frac{1-\eta}{\tau}}, \quad F = \frac{g_{\mathrm{m}}\, \mathbf{K}_f}{\kappa\, \mathbf{K}_3}\sqrt{\frac{4\Gamma_m}{\kappa\tau}}, \end{aligned} \tag{A16}$$

$$\begin{aligned} &H = \left(\mathbf{K}_f\sqrt{\frac{2\eta}{\kappa\tau}}(1 - \mathrm{e}^{-\kappa\tau}(2\kappa\tau + 1)) - g_{\mathrm{a}}\frac{(1 - \mathrm{e}^{-\kappa\tau})}{\kappa}\right), \\ &J = \mathbf{K}_f\sqrt{\frac{2}{\kappa\tau}}(1 - \mathrm{e}^{-\kappa\tau}), \end{aligned} \tag{A17}$$

$$\begin{aligned} &L = -g_{\mathrm{m}}\frac{1 - e^{-\kappa\tau}}{\kappa}, \quad M = -\sqrt{2\kappa\eta}\, \frac{g_{\mathrm{m}}}{\kappa \mathbf{K}_6}, \\ &R = -2\sqrt{\eta}\, g_{\mathrm{m}}\frac{(1 - \mathrm{e}^{-\kappa\tau}(1 + \kappa\tau))}{\kappa}, \quad U = -\frac{g_{\mathrm{m}}}{\mathbf{K}_2}\sqrt{\frac{2(1-\eta)}{\kappa}}. \end{aligned} \tag{A18}$$

The canonical variables (boldface) used to define the noise terms are as follows. The thermal noise of the mechanical environment is described by $(\hat{\boldsymbol{\zeta}}^{X_m}, \hat{\boldsymbol{\zeta}}^{P_m}, \hat{\boldsymbol{\zeta}}_f^{X_m}, \hat{\boldsymbol{\zeta}}_f^{P_m})$. The input light pulse is described by $(\hat{\mathbf{X}}^{\text{in}}, \hat{\mathbf{P}}^{\text{in}}, \hat{\mathbf{X}}_f^{\text{in}}, \hat{\mathbf{P}}_f^{\text{in}})$. The vacuum admixed by optical losses: $(\hat{\mathbf{X}}^{\text{vac}}, \hat{\mathbf{P}}^{\text{vac}})$. The initial values of the intracavity optical light $(\hat{\mathbf{X}}_0, \hat{\mathbf{P}}_0)$ and $(\hat{\mathbf{X}}_0', \hat{\mathbf{P}}_0')$. The formal definitions of these canonical quadratures read

$$\hat{\boldsymbol{\zeta}}^{X_m,P_m} = \frac{1}{\sqrt{\tau 2\Gamma_{\text{M}}}}\int_0^\tau dt\ \hat{\zeta}_{\text{X}_\text{M},\text{P}_\text{M}}(t),$$

$$\hat{\mathbf{X}}^{\text{vac}} = \mathbf{K}_1(f_1(\tau) * \hat{x}_{\text{vac}}(\tau)), \tag{A19a}$$

$$\hat{\boldsymbol{\zeta}}_f^{X_m} = \frac{\mathbf{K}_3}{\sqrt{2\Gamma_{\text{M}}}}(f_3 * \hat{\zeta}_{X_\text{M}})(\tau),$$

$$\hat{\mathbf{P}}^{\text{vac}} = \mathbf{K}_2(f_2 * \hat{p}_{\text{vac}})(\tau), \tag{A19b}$$

$$\hat{\mathbf{X}}^{\text{in}} = \mathbf{K}_2(f_2 * \hat{x}_{\text{in}})(\tau), \quad \hat{\mathbf{X}}_{\text{f}}^{\text{in}} = \mathbf{K}_5(f_5 * \hat{x}_{\text{in}})(\tau), \tag{A19c}$$

$$\hat{\mathbf{P}}^{\text{in}} = \mathbf{K}_6(f_6 * \hat{p}_{\text{in}})(\tau), \tag{A19d}$$

with the following definitions:

$$f_1(t) = 1 - 2\text{e}^{-\kappa t}, \quad f_2(t) = 1 - \text{e}^{-\kappa t},$$
$$f_3(t) = \kappa t - 1 + \text{e}^{-\kappa t}, \quad f_5(t) = 1 - 4\kappa t\,\text{e}^{-\kappa t},$$
$$f_6(t) = 1 - \text{e}^{-\kappa t}(2\kappa t + 1),$$
$$\mathbf{K}_i = \left(\int_0^\tau f_i^2(t)dt\right)^{-1/2}, \quad \mathbf{K}_{ij} = \left(\int_0^\tau f_i(t)f_j(t)dt\right)^{-1/2},$$
$$i, j = 1, 2, 3, 5, 6.$$

Also,

$$\mathbf{K}_f = \frac{\sqrt{2\eta\tau}g_{\text{a}}(\text{e}^{-\kappa\tau}(\kappa\tau + 2) + \kappa\tau - 2)}{\sqrt{\kappa}(\kappa\tau - 1 + \text{e}^{-\kappa t})},$$

$$\mathbf{K}_4 \equiv \left(\int_0^\tau f_3(t)dt\right)^{-1/2} = \frac{2(1-\kappa\tau) - 2\text{e}^{-\kappa\tau} + \kappa^2\tau^2}{2\kappa},$$

$$\mathbf{K}_7 \equiv \frac{1}{\mathbf{K}_{25}} = \frac{2\text{e}^{-\kappa\tau}(3 + 2\kappa\tau) + (\kappa\tau - 4) - 2\text{e}^{-2\kappa\tau}(1 + 2\kappa\tau)}{\kappa}.$$

Above, the asterisk $(*)$ denotes convolution:

$$(f * g)(t) \equiv \int_0^t f(t-s)g(s)\text{d}s\,. \tag{A20}$$

Finally, we have to specify the statistics of the modes we defined above. All the canonical quadratures defined so far (boldface), except the initial mechanical and atomic states, describe Gaussian vacuum or thermal states. The initial mechanical and atomic states are in coherent states, that is, Gaussian states with nonzero initial mean values and covariance matrices equal to 2×2 identity matrix $\mathbb{1}_2$. See Sec. IV for a brief overview of the necessary Gaussian toolbox, including the definition of the covariance matrices that we use. The input light and the noise modes have the following nonzero covariances (defined as $\langle a, b\rangle_s = \frac{1}{2}\langle ab + ba\rangle$):

$$\langle \hat{x}_{\text{in}}(t), \hat{x}_{\text{in}}(t')\rangle_s = \frac{1}{S}\delta(t - t'),$$
$$\langle \hat{p}_{\text{in}}(t), \hat{p}_{\text{in}}(t')\rangle_s = S\delta(t - t'), \tag{A21}$$

$$\langle \hat{x}_{\text{vac}}(t), \hat{x}_{\text{vac}}(t')\rangle_s = \langle \hat{p}_{\text{vac}}(t), \hat{p}_{\text{vac}}(t')\rangle_s = \delta(t - t'), \tag{A22}$$

$$\langle \hat{\zeta}_{X_\text{M}}, \hat{\zeta}_{X_\text{M}}\rangle_s = \langle \hat{\zeta}_{P_\text{M}}, \hat{\zeta}_{P_\text{M}}\rangle_s = (2n_{\text{th}} + 1)\delta(t - t'). \tag{A23}$$

Using these relations and Eqs. (A19), we can compute the covariances of the canonical modes (boldface) in Eqs. (A19), of which the following are nonzero:

$$\begin{aligned}\langle \hat{\boldsymbol{\zeta}}_f^{X_\text{m}}, \hat{\boldsymbol{\zeta}}_f^{X_\text{m}}\rangle &= \langle \hat{\boldsymbol{\zeta}}^{X_\text{m}}, \hat{\boldsymbol{\zeta}}^{X_\text{m}}\rangle = \langle \hat{\boldsymbol{\zeta}}^{P_\text{m}}, \hat{\boldsymbol{\zeta}}^{P_\text{m}}\rangle \\ &= \langle \hat{\mathbf{X}}^{\text{in}}, \hat{\mathbf{X}}^{\text{in}}\rangle = \langle \hat{\mathbf{P}}^{\text{in}}, \hat{\mathbf{P}}^{\text{in}}\rangle = \langle \hat{\mathbf{X}}_f^{\text{in}}, \hat{\mathbf{X}}_f^{\text{in}}\rangle = 1,\end{aligned} \tag{A24}$$

$$\langle \hat{\boldsymbol{\zeta}}^{X_\text{m}}, \hat{\boldsymbol{\zeta}}_f^{X_\text{m}}\rangle_s = \langle \hat{\boldsymbol{\zeta}}^{P_\text{m}}, \hat{\boldsymbol{\zeta}}_f^{P_\text{m}}\rangle_s = \frac{\mathbf{K}_3\mathbf{K}_4}{\sqrt{\tau}},$$
$$\langle \hat{\mathbf{X}}^{\text{in}}, \hat{\mathbf{X}}_f^{\text{in}}\rangle_s = \langle \hat{\mathbf{P}}^{\text{in}}, \hat{\mathbf{P}}_f^{\text{in}}\rangle_s = \frac{\mathbf{K}_2\mathbf{K}_5}{\mathbf{K}_{25}}. \tag{A25}$$

2. Output classical threshold and nonclassicality threshold

In this section, we introduce the thresholds we use in the paper to distinguish nonclassical coincidences of excitations in the quantum system. To devise the thresholds, we adhere to the convention according to which nonclassical are such states for which the Glauber-Sudarshan P function is not a regular probability distribution [57]. We therefore make extensive use of the properties of coherent states for our thresholds. In particular, we use that for a coherent state α, the probabilities $p_k = |\langle k|\alpha\rangle|^2$ can all be expressed in terms of the probability p_0. For instance, the single-photon contribution for a coherent state given its vacuum contribution p_0 equals

$$p_1^{\text{c}}(p_0) = p_0 \ln\frac{1}{p_0}. \tag{A26}$$

This probability is bounded by $p_1^{\text{c}}(p_0) \leqslant \text{e}^{-1}$. This allows us to immediately devise the *output classical threshold* $F_{00} = \text{e}^{-2}$ as the maximal element p_{11} attainable by bipartite states that are mixtures of coherent states.

We use a less stringent threshold $F_{11}(\rho)$ defined as the maximal p_{11} contribution attainable by coherent states that have the same vacuum contribution p_0 as state ρ. To formally define this threshold, first, let us introduce notation for certain photon-number contributions of single-mode quantum states:

$$\mathcal{P}_k(\rho) = \langle k|\rho|k\rangle. \tag{A27}$$

The threshold $F_{11}(\rho)$ is then defined as a function of the state as follows:

$$F_{11}(\rho) \equiv p_1^{\text{c}}[\mathcal{P}_0(\text{Tr}_b\rho)] \times p_1^{\text{c}}[\mathcal{P}_0(\text{Tr}_a\rho)]. \tag{A28}$$

The threshold F_{11} is defined using the probabilities p_1^{c} that correspond to pure coherent states. Below we prove that this threshold represents the maximal value of the element p_{11} achievable by classical states with equivalent vacuum contributions. That is,

$$F_{11}(\rho_a \otimes \rho_b) \geqslant \max_{\rho_a,\rho_b} \mathcal{P}_1(\rho_a)\mathcal{P}_1(\rho_b), \tag{A29}$$

with $\rho_{a,b}$ both being classical, that is, admitting a representation in the form

$$\rho_{\text{cl}} = \int \text{d}^2\alpha\, P(\alpha)|\alpha\rangle\langle\alpha|, \quad \text{d}^2\alpha \equiv \text{d Re}\alpha\ \text{d Im}\alpha, \tag{A30}$$

with $P(\alpha)$ being a regular probability density function, and $\mathcal{P}_0(\rho_a) = \mathcal{P}_0(\mathrm{Tr}_b\rho)$ and $\mathcal{P}_0(\rho_b) = \mathcal{P}_0(\mathrm{Tr}_a\rho)$.

Note that classical states admit no quantum entanglement and hence it is sufficient to prove Eq. (A29) in this exact form (for product states) to show that F_{11} is indeed the upper boundary of the probability p_{11} for classical states. From Eq. (A29) it follows that we have to prove that the maximal single-photon contribution achievable by classical states that have a certain vacuum contribution is attained by a pure coherent state. Importantly, it is sufficient to prove this for a single-mode case, since the generalization for product states (that cover all possible classical states) is trivial.

The zero-photon (vacuum) contribution of a classical state is

$$\mathcal{P}_0(\rho_{\mathrm{cl}}) = \int \mathrm{d}^2\alpha\, P(\alpha) r(\alpha), \quad \text{where } r(\alpha) \equiv |\langle 0|\alpha\rangle|^2. \tag{A31}$$

The single-photon contribution of the state (A30) is

$$\mathcal{P}_1(\rho_{\mathrm{cl}}) = \int \mathrm{d}^2\alpha\, P(\alpha) r(\alpha) \ln \frac{1}{r(\alpha)}. \tag{A32}$$

At the same time, a pure coherent state with the same vacuum contribution $\mathcal{P}_0(\rho_{\mathrm{cl}})$ would have a single-photon contribution equal to

$$p_1^{\mathrm{c}}[\mathcal{P}_0(\rho_{\mathrm{cl}})] = \mathcal{P}_0(\rho_{\mathrm{cl}}) \ln \frac{1}{\mathcal{P}_0(\rho_{\mathrm{cl}})}. \tag{A33}$$

Our goal is to prove that

$$\delta p \equiv p_1^{\mathrm{c}}[\mathcal{P}_0(\rho_{\mathrm{cl}})] - \mathcal{P}_1(\rho_{\mathrm{cl}}) \geqslant 0. \tag{A34}$$

By construction of a classical state, $P(\alpha)$ is a regular probability density and thus $P(\alpha)\mathrm{d}^2\alpha$ is a probability measure. Therefore, we can rewrite

$$\delta p = \left[\int \mathrm{d}^2\alpha\, P(\alpha) r(\alpha)\right] \times \ln \frac{1}{\int \mathrm{d}^2\alpha\, P(\alpha) r(\alpha)} - \int \mathrm{d}^2\alpha\, P(\alpha) r(\alpha) \ln \frac{1}{r(\alpha)} \tag{A35}$$

as

$$\delta p = p_1^{\mathrm{c}}(\mathbb{E}[r(\alpha)]) - \mathbb{E}\big[p_1^{\mathrm{c}}(r(\alpha))\big], \tag{A36}$$

where $\mathbb{E}[\cdot]$ means taking the expectation value. The function $p_1^{\mathrm{c}}(x)$ is defined for $0 \leqslant x \leqslant 1$ where it is concave. Therefore, it follows from Jensen's inequality [91] that

$$p_1^{\mathrm{c}}(\mathbb{E}[r(\alpha)]) \geqslant \mathbb{E}\big[p_1^{\mathrm{c}}(r(\alpha))\big], \quad \text{and hence } \delta p \geqslant 0. \tag{A37}$$

The threshold $F_{11}(\rho)$, therefore, shows the maximal element p_{11} possible to achieve with *all classical states* (regular mixtures of coherent states) that possess the same vacuum contributions as state ρ.

The advantage of a certain state's element p_{11} over the threshold F_{11} is the main figure of merit of our protocol:

$$\Delta(\rho) = \max[0, p_{11}(\rho) - F_{11}(\rho)]. \tag{A38}$$

By analogy with F_{11}, we can devise similar thresholds for higher Fock-state contributions, e.g., for the contribution

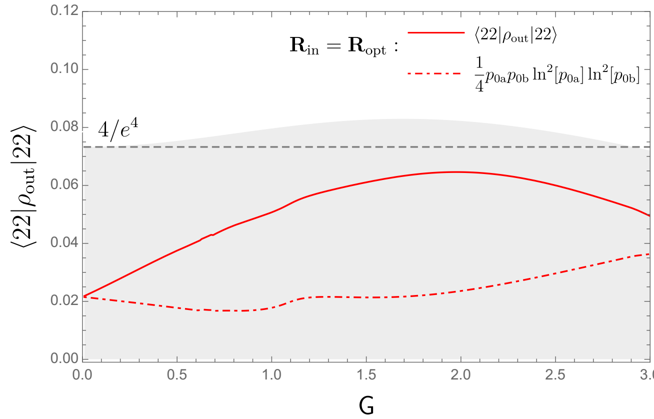

FIG. 5. Nonclassical coincidences of pairs of excitations at the output of a unitary QND gate with classical input, evaluated via p_{22}. Gray shaded area shows all possible values of p_{22} attainable at the output. Solid and dashed red lines show, respectively, the p_{22} element and the corresponding threshold F_{22} for the state that maximizes the difference between them for a given gain. Optimization is performed over the quadrature amplitudes of the input coherent states.

$p_{22} = \langle 22|\rho|22\rangle$ or, in general, for $p_{nn} = \langle nn|\rho|nn\rangle$:

$$F_{nn}(\rho) \equiv p_n^{\mathrm{c}}[\mathcal{P}_0(\mathrm{Tr}_b\rho)] \times p_n^{\mathrm{c}}[\mathcal{P}_0(\mathrm{Tr}_a\rho)], \quad \text{where}$$
$$p_n^{\mathrm{c}}(x) = \frac{x}{n!} \cdot (-\ln x)^n. \tag{A39}$$

Homodyne detection allows reconstruction of the covariance matrix of the output Gaussian state. This, in turn, allows us to estimate all the contributions p_k of the state. In particular, in Fig. 5 we illustrate the nonclassical coincidences in the form of p_{22} generated by a QND transformation of the input coherent states. The output classical threshold for this probability equals $4\mathrm{e}^{-4}$. The threshold is given by Eq. (A39) with $n = 2$ and is shown to be possible to overcome given optimized input coherent states.

To summarize, the full step-by-step recipe to compute $F_{11}(\rho)$ is as follows:

(1) Given a bipartite state of atoms (a) and mechanics (m) ρ, we compute the partial states by tracing out the other subsystem:

$$\rho_{\mathrm{a}} = \mathrm{Tr}_{\mathrm{m}}\rho; \quad \rho_{\mathrm{m}} = \mathrm{Tr}_{\mathrm{a}}\rho. \tag{A40}$$

(2) The partial states allow computing the vacuum contributions of individual subsystems:

$$p_{0\mathrm{a}} = \langle 0|\rho_{\mathrm{a}}|0\rangle; \quad p_{0\mathrm{m}} = \langle 0|\rho_{\mathrm{m}}|0\rangle. \tag{A41}$$

(3) Taking the product of maximal single-photon contributions p_1^{c} that correspond to the given vacuum contributions yields F_{11} for state ρ:

$$F_{11}(\rho) = p_1^{\mathrm{c}}(p_{0\mathrm{a}}) p_1^{\mathrm{c}}(p_{0\mathrm{m}}). \tag{A42}$$

3. Performance of a unitary qnd gate

To further discuss the performance of the gate, here we compare a realistic gate with the case of a unitary gate with the decoherence absent. This latter case is a convenient example model because it allows a compact analytical solution thanks to the Gaussian nature of the input states and interactions (see Appendix 4 for details).

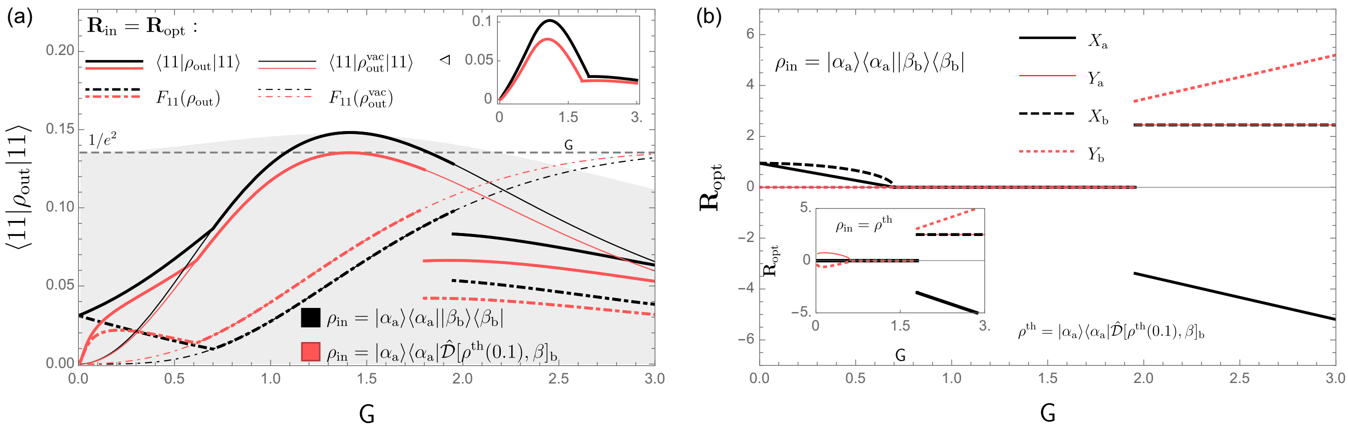

FIG. 6. (a) Nonclassical coincidences $\langle 11|\rho_{\rm out}|11\rangle$ (solid curves) and nonclassicality thresholds $F_{11}(\rho_{\rm out})$ (dot-dashed curves) calculated for the output state of a unitary QND gate with a classical input, as a function of the gate gain. Black curves are calculated for the case of coherent states in both input ports, red curves assume a coherent state in one port and a displaced thermal state in another, as a model of a coherent state influenced by thermal noise. Thick curves are calculated with the vector of means of the input state providing maximal $\Delta \equiv \langle 11|\rho_{\rm out}|11\rangle - F_{11}(\rho_{\rm out})$ (traced in the inset as a function of the gain G). Thin curves correspond to the case of vacuum at the input in both modes. Gray area corresponds to all values of p_{11} attainable at the output with classical input. (b) Quadrature amplitudes of the input coherent states that deliver optimal Δ in (a). In the inset, the optimal mean input quadratures for a displaced thermal state in one input port and a coherent state at another. Due to the phase-insensitive figure of merit, the optimal input states are not unique.

An ideal QND gate, characterized by the unitary propagator $U_{\mathsf{G}} = \exp[\mathsf{G}(a + a^\dagger)(b^\dagger - b)/2]$, describes an active evolution of two oscillators described by the ladder operators a and b. In the case of unitary interaction, the interaction gain G is the only parameter characterizing the gate. In this section, we analyze the action of the gate on classical inputs $\rho_{\rm in}$ by evaluating the corresponding output states $\rho_{\rm out} = U_{\mathsf{G}}\rho_{\rm in}U_{\mathsf{G}}{}^\dagger$. Of main interest are different-number photon contributions of this output state, i.e., the main diagonal matrix elements $p_{nm} = \langle n_{\rm a}m_{\rm b}|\rho_{\rm out}|n_{\rm a}m_{\rm b}\rangle$ that show the probability to detect $n_{\rm a}$ photons in one mode and $m_{\rm b}$ in the other one. To evaluate the nonclassicality of the output state, we will focus on its p_{11} contribution, comparing it with two thresholds equal to the p_{11} reachable by certain classes of classical states: First, the absolute classical threshold $F_0 = 1/e^2$, which is the maximal probability attainable by arbitrary classical statesand, second, the output classical threshold F_{11} defined by Eq. (9).

First, let us consider input vacuum, which is the trivial classical state $\rho^{\rm vac} \equiv |0_{\rm a}0_{\rm b}\rangle\langle 0_{\rm a}0_{\rm b}|$. At input, for this state all the matrix elements are zero except $p_{00}^{\rm vac} = 1$. A passive transformation, conserving the total number of excitations, would map the initial vacuum state onto itself. This is not so for the QND gate with vacuum input. A QND gate performs an active transformation and creates (and annihilates) excitations in pairs, as follows from its expansion in the ladder operators. Thereby, the probability of detecting arbitrary numbers of excitations in two modes that sum to an even numbe, becomes nonzero and functions of the interaction gain. Importantly, in the unitary case with vacuum input, the contributions p_{ij} can be derived analytically. For a relatively low gain $\mathsf{G} \lessapprox 1$, the output state remains mostly the two-mode vacuum with a minute addition of $|11\rangle$ state, as follows from Eq. (A43). As the gain increases, the output state is predominantly formed by the contributions of states with at most two excitations: $|00\rangle$, $|11\rangle$, $|20\rangle$, and $|02\rangle$ For moderate values of the gain $\mathsf{G} \lessapprox \sqrt{2}$, these states contribute about 90% of the total probability: $p_{00} + p_{11} + p_{20} + p_{02} \approx 0.9$. Note that p_{11} has a well-pronounced maximum at $\mathsf{G} = \sqrt{2}$: $p_{11}(\sqrt{2}) = 4/27$. The unitary gate thus turns the input vacuum state into a state with the p_{11} contribution exceeding the absolute threshold F_0, and hence nonclassical. One can see that the threshold is surpassed by only a small amount and thereby a more sensitive threshold can be required to verify the nonclassicality in p_{11}. As a path to a more sensitive figure of merit, we devise a less restrictive threshold, that is, the output threshold F_{11} which is also possible to overcome starting with vacuum.

Next, let us investigate products of coherent states at the input $\rho_{\rm in} = \rho^{\rm coh} = |\alpha\rangle\langle\alpha| \otimes |\beta\rangle\langle\beta|$, which correspond to a more general case of classical states. The output state, corresponding to the input coherent ones, is fully defined by the five real numbers which include the four mean values of the quadratures at input, and the interaction gain. Optimization over the input parameters to maximize the p_{11} for each gain G allows us to determine the values reachable at the output. These values are shown by the gray area in Fig. 6. The absolute maximum of p_{11} is reached by vacuum input that happens to be a subset of product coherent states. Overall, the output states from coherent input do not provide a strong advantage over the absolute threshold F_0. To fully cover this class, we perform the optimization of the advantage Δ defined in Eq. (10) over all possible coherent states at input. The result of the optimization is in Fig. 6, where we show the contribution p_{11} and the threshold value F_{11} in the main panel and the advantage Δ in the inset.

Finally, to analyze the imperfections in state preparation, we illustrate the presence of thermal noise in the system by admixing the thermal state to one of the input ports. Admixture of a thermal state to a coherent state results in attenuation of the coherent state mean quadratures and increase of the quadrature variances. The resulting state thus can be written as $\hat{\mathcal{D}}[\rho_{\rm th}(n), \alpha]$. It is a thermal state with mean occupation n displaced by vector $\mu_D = (\alpha + \alpha^*, {\rm i}(\alpha^* - \alpha))$ in the phase space. This state is Gaussian and can be characterized by the vector of means μ_D and covariance matrix $V_{\rm th}(n) = (2n+1)\mathbb{1}_2$ (where $\mathbb{1}_2$ is a 2×2 identity matrix). The thermal state of mean occupation n can be expanded in the Fock-state basis as $\rho_{\rm th}(n) = (1+n)^{-1}\sum(1+n^{-1})^{-k}|k\rangle\langle k|$. The input state is thus $\rho_{\rm in} = \hat{\mathcal{D}}[\rho_{\rm th}(n),\alpha]\otimes|\beta\rangle\langle\beta|$. Given a certain value of n, for each value of G the output state is determined by four numbers that define α and β. After optimization over these numbers, it is possible to conclude that, quite predictably, an admixture of thermal noise causes a decrease in both reachable advantage Δ and the contribution p_{11}. Compared to pure coherent states at the input, mixed states can no longer overcome the absolute threshold F_0. It is possible to overcome F_{11}, however, the value of the advantage Δ is reduced. Additionally, in comparison with the pure input, the maximal value of G where the vacuum input gives the best advantage is reduced. This is apparently because, due to the larger occupation in the initial state, the strategy of redistribution the excitations becomes optimal at smaller interaction gain.

Importantly, if noise is relatively small, it is possible to find the optimal initial state that gives a positive advantage Δ for each G. However, for $p=0$ (i.e., for a thermal state at one of the input ports), the output state shows positive advantage Δ only in a very small range of thermal excitations, approximately for $n \lessapprox 0.7$ (using vacuum at the other input). For any $p>0$, there are certain values of the gain (depending also on n) that provide positive Δ.

The values of gain $\mathfrak{G}$ at which the switching takes place are mostly determined by the mean occupation of the initial state of the input modes and the noise added by interaction. A simple illustrative picture is qualitatively given by expansion of Eq. (6) to the first order in the interaction gain:

$$\hat{\mathcal{U}} \approx \mathbb{1} + \mathfrak{G}(\hat{a}_{\rm M}+\hat{a}_{\rm M}^\dagger)(\hat{a}_{\rm A}-\hat{a}_{\rm A}^\dagger). \tag{A43}$$

The evolution provided by the gate involves an intricate interference of the excitation hopping process ($a_{\rm M}a_{\rm A}^\dagger$) and two-mode squeezing ($a_{\rm M}^\dagger a_{\rm A}^\dagger$). The former creates pairs of excitations and thus is the one directly contributing to the figure of merit p_{11} (given the initial vacuum state). For this contribution to be substantial, a sufficiently large gain $\mathfrak{G}$ is required. Therefore, the region having vacuum as the initial state appears to be optimal only for sufficiently large values of the gain. For smaller values of the gain, a more successful strategy to increase p_{11} is to enhance it by redistribution of the initial occupation via the excitations hopping. The optimal initial state for small $\mathfrak{G}$ is thereby a state with nonzero mean occupation. By similar logic, for high values of $\mathfrak{G}$, the optimal strategy to enhance p_{11} is to redistribute the initial occupations.

The output of a unitary QND gate can be conveniently used to illustrate the role of the numerical value of Δ. The magnitude of this advantage is related to the magnitude of nonclassicality. In particular, Fig. 7 illustrates how Δ changes under attenuation and admixture of thermal noise. To show this, we start with the bipartite state $\rho_{\rm qnd}(\mathsf{G}) = U_{\mathsf{G}}|\alpha\rangle\langle\alpha|\otimes|\beta\rangle\langle\beta|U_{\mathsf{G}}^\dagger$, where α and β are such that yield maximal $\Delta[\rho_{\rm qnd}(\mathsf{G})]$. That is, $\rho_{\rm qnd}$ is the output state of a unitary QND gate with gain G, with optimal coherent states at the input. Each party of this state is assumed to be attenuated by a factor of η with an admixture of thermal noise. For simplicity,

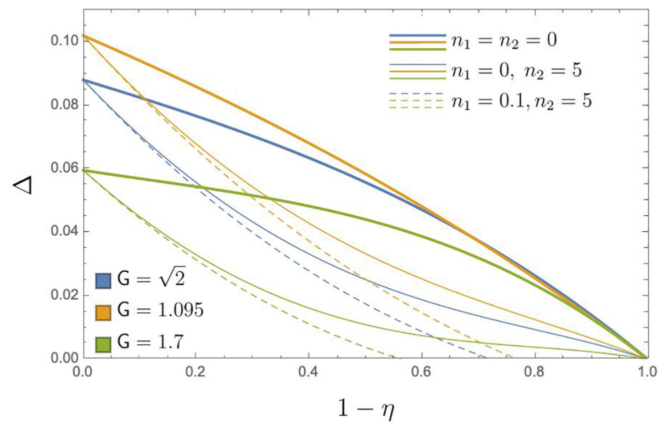

FIG. 7. Decrease of the nonclassicality witness Δ caused by attenuation (denoted η; $1-\eta=0$ corresponds to no attenuation) and admixture of noise. Different colors correspond to different preattenuation states. Different dashing corresponds to different added noise.

we assume equal attenuation of both modes. Denoting the quadratures of our bipartite system as (X_1,P_1) and (X_2,P_2), in the Heisenberg picture, the admixture of noise is described by

$$\begin{aligned} X_1 &\mapsto X_1' = \sqrt{\eta}X_1 + \sqrt{1-\eta}X_{N_1},\\ P_1 &\mapsto P_1' = \sqrt{\eta}P_1 + \sqrt{1-\eta}P_{N_1},\\ X_2 &\mapsto X_2' = \sqrt{\eta}X_2 + \sqrt{1-\eta}X_{N_2},\\ P_2 &\mapsto P_2' = \sqrt{\eta}P_2 + \sqrt{1-\eta}P_{N_2}, \end{aligned}$$

where $(X,P)_{N_{(A,B)}}$ are quadratures of the noise modes with covariances

$$\langle X_{N_i}, X_{N_i}\rangle_s = \langle P_{N_i}, P_{N_i}\rangle_s = 2n_i + 1. \tag{A44}$$

Or, equivalently, we can write the state with admixed noise as

$$\begin{aligned} \rho_{\rm qnd}'(\mathsf{G},\eta,n_1,n_2) = U_{\rm BS1}U_{\rm BS2}[\rho_{\rm qnd}(\mathsf{G})\otimes\rho_{\rm th}(n_1)\\ \otimes\rho_{\rm th}(n_2)]U_{\rm BS2}^\dagger U_{\rm BS1}^\dagger, \end{aligned}\tag{A45}$$

where $U_{\rm BSi}$ denotes a beam-splitter operation with transmissivity η between the modes with quadratures (X_i,P_i) and (X_{N_i},P_{N_i}).

In Fig. 7, we show $\Delta(\rho_{\rm qnd}')$ as a function of the attenuation η for different values of the gain G and occupations n_i of the noise modes. Clearly, with increasing attenuation by pure loss (admixture of vacuum), Δ reduces until eventually it vanishes when the attenuation reaches 100%. If the attenuation is accompanied by an admixture of thermal noise instead of a vacuum, Δ decreases faster and becomes zero at a finite value of η.

4. Brief overview of gaussian formalism

In this paper, we investigate the QND gates with the classical input states and demonstrate nonclassicality of the resulting output state using its single-photon contribution. Importantly, the classical input states belong to the class of Gaussian states, and the QND gate, being linear, transforms them into other Gaussian states. Therefore, to describe the action of the gate on classical states, it is sufficient to use Gaussian formalism. In this section, we first provide the material concerning this formalism, sufficient to make our treatment self-consistent. Then, we separately illustrate a method to evaluate the single-photon contribution of Gaussian states because the single-photon state is not Gaussian. A more comprehensive review of Gaussian states and maps can be found, e.g., in Refs. [92,93].

Gaussian quantum states can be defined as such states whose Wigner functions are Gaussian functions of the phase-space variables. These states have the advantage of the theoretical description that the full information about them is contained in the first two statistical moments. If a system is described, in the Heisenberg picture, by a vector of quadratures $\mathbf{r}$, these first two statistical moments are the vector of mean values $\mu = \langle \mathbf{r} \rangle$ and the covariance matrix V with elements ($a \circ b \equiv (ab + ba)/2$ is the Jordan product)

$$V_{ij} = \langle (r_i - \mu_i) \circ (r_j - \mu_j) \rangle. \tag{A46}$$

Here the averaging is understood in quantum mechanical sense $\langle A \rangle = \mathrm{Tr}(A\rho)$, where ρ is the Gaussian quantum state whose statistical moments are being computed.

We use at the input coherent states for which (in the single-mode case) $\mu^{\mathrm{coh}} = (x, y), x, y \in \mathbb{R}$, and CM is an identity matrix $V^{\mathrm{coh}} = \mathbb{1}_2$. We also use thermal states which have zero means $\mu^{\mathrm{th}} = \mathbf{0}$ but larger variances $V^{\mathrm{th}} = (2n_{\mathrm{th}} + 1)\mathbb{1}_2$, with n_{th} being mean occupation. The vacuum state can be represented as a thermal with $n_{\mathrm{th}} = 0$ or, equivalently, a coherent state with zero means $\mu^{\mathrm{vac}} = \mathbf{0}$. Single-mode- and two-mode-squeezed states (SMS and TMS, respectively) have zero means and more complicated covariance matrices:

$$V^{\mathrm{SMS}} = \begin{pmatrix} \cosh 2r + \cos 2\varphi \sinh 2r & \sin 2\varphi \sinh 2r \\ \sin 2\varphi \sinh 2r & \cosh 2r - \cos 2\varphi \sinh 2r \end{pmatrix}, \tag{A47}$$

$$V^{\mathrm{TMS}} = \begin{pmatrix} \cosh(2r) \cdot \mathbb{1}_2 & \sinh(2r) \cdot \bar{\sigma}_3 \\ \sinh(2r) \cdot \bar{\sigma}_3 & \cosh(2r) \cdot \mathbb{1}_2 \end{pmatrix},$$
$$\text{where } \bar{\sigma}_3 = \begin{pmatrix} -\sin\varphi & -\cos\varphi \\ -\cos\varphi & \sin\varphi \end{pmatrix}. \tag{A48}$$

The parameter r describes the squeezing magnitude, φ, the tilt of the squeezing direction. Finally, a displaced squeezed state $\mathrm{DS}|0\rangle$ is characterized by the vector of means μ defined by the displacement operator, and the covariance matrix analogous to V^{SMS}.

Multipartite product Gaussian states can be assembled from the Gaussian states of the partitions by taking a direct matrix sum of the moments: $\mu^{(1+2)} = \mu^{(1)} \oplus \mu^{(2)}, V^{(1+2)} = V^{(1)} \oplus V^{(2)}$.

Physical interactions characterized by Hamiltonian operators that are up to quadratic in the system quadrature operators preserve the Gaussian character of the states. Such interactions can be described by input-output relations that are linear in quadrature operators. Importantly, the Heisenberg-Langevin equations needed to describe the atom-opto-mechanical system generate such input-output relations. If before the interaction the vector of quadratures is $\mathbf{r}^{\mathrm{in}}$, after the interaction it is $\mathbf{r}^{\mathrm{out}}$, expressed as

$$\mathbf{r}^{\mathrm{out}} = T\mathbf{r}^{\mathrm{in}} + \mathbf{N}, \tag{A49}$$

where $\mathbf{N}$ is a vector of noise terms introduced by the interaction. Substituting this equation into the definitions of the statistical moments of quadratures allows us to immediately find how they evolve in the interaction

$$\mu^{\mathrm{out}} = T\mu^{\mathrm{in}}, \quad V^{\mathrm{out}} = TV^{\mathrm{in}}T^{\top} + V_N, \tag{A50}$$

where V_N is the covariance matrix related to the noise $\mathbf{N}$ (assuming these noise terms are Gaussian as well). A particularly convenient property of Gaussian channels is that the transformations induced by them are linear. That is, if the channel performs a map $\rho_{\mathrm{in}} \mapsto \rho_{\mathrm{out}} = \mathcal{T}[\rho_{\mathrm{in}}]$, its action can be distributed over mixtures of Gaussian states:

$$\mathcal{T}\left[\sum_i p_i \rho_i\right] = \sum_i p_i \mathcal{T}[\rho_i]. \tag{A51}$$

The transformation corresponding to the QND interaction described by Eqs. (1) to (4) is characterized by the matrix T that reads

$$T = \begin{pmatrix} 1 & 0 & -\mathfrak{G} & 0 \\ 0 & 1 & 0 & 0 \\ 0 & 0 & 1 & 0 \\ \mathfrak{G} & 0 & 0 & 1 \end{pmatrix}. \tag{A52}$$

The complete expressions for the elements V_N are too cumbersome to be reported here.

Other paradigmatic Gaussian transformations include the beam splitter (BS) and two-mode-squeezing, or amplification (AMP), transformations. The corresponding Hamiltonian operators $H_{\mathrm{BS}} = \Theta\hbar i(a^\dagger b - b^\dagger a)$, and $H_{\mathrm{AMP}} = \Phi\hbar i(a^\dagger b^\dagger - ab)$ allow us to derive the transformation matrices T:

$$T_{\mathrm{BS}} = \begin{pmatrix} \sqrt{\mathsf{T}} & 0 & \sqrt{1-\mathsf{T}} & 0 \\ 0 & \sqrt{\mathsf{T}} & 0 & \sqrt{1-\mathsf{T}} \\ -\sqrt{1-\mathsf{T}} & 0 & \sqrt{\mathsf{T}} & 0 \\ 0 & -\sqrt{1-\mathsf{T}} & 0 & \sqrt{\mathsf{T}} \end{pmatrix},$$
$$T_{\mathrm{AMP}} = \begin{pmatrix} \sqrt{\mathsf{A}} & 0 & \sqrt{\mathsf{A}-1} & 0 \\ 0 & \sqrt{\mathsf{A}} & 0 & \sqrt{\mathsf{A}-1} \\ \sqrt{\mathsf{A}-1} & 0 & \sqrt{\mathsf{A}} & 0 \\ 0 & \sqrt{\mathsf{A}-1} & 0 & \sqrt{\mathsf{A}} \end{pmatrix}. \tag{A53}$$

Here, for the BS, $\mathsf{T} \equiv \cos^2[\Theta]$ is a transmittance coefficient; for the AMP, $\mathsf{A} \equiv \cosh^2[\Phi]$ describes amplification gain.

Gaussian states have a convenient representation using WFs [94,95]. A single-mode WF takes two real numbers $\mathbf{r} = (x, y)$ that correspond to a point in the phase space as arguments and shows the quasiprobability density distribution. In general, the WF corresponding to an operator σ reads

$$W_\sigma(x, p) = \frac{1}{2\pi} \int_{-\infty}^{+\infty} \mathrm{d}y\, \langle x + y|\sigma|x - y\rangle \mathrm{e}^{-\mathrm{i}py}. \tag{A54}$$

A Gaussian state with means μ and covariance matrix V has the Wigner function equal to

$$W(\mathbf{r}) = \mathsf{W}(\mathbf{r}; \mu, V) \equiv \frac{1}{4\pi^2\sqrt{\det V}} \exp\left(-\frac{1}{2}(\mathbf{r} - \mu)^T V^{-1}(\mathbf{r} - \mu)\right). \tag{A55}$$

Using the formalism of WFs, it is possible to efficiently compute the matrix elements of interest. This is because for bipartite quantum states ρ and σ:

$$\mathrm{Tr}(\rho\sigma) = (4\pi)^2 \int \mathrm{d}^4\mathbf{r}\, W_\rho(\mathbf{r}) W_\sigma(\mathbf{r}). \tag{A56}$$

Using this identity, it is possible to write

$$\begin{aligned}\langle 11|\rho|11\rangle &= \mathrm{Tr}[\rho(|1\rangle\langle 1|_a \otimes |1\rangle\langle 1|_b)] \\ &= (4\pi)^2 \int \mathrm{d}x\, \mathrm{d}y\, \mathrm{d}q\, \mathrm{d}p\, W_\rho(x, y, q, p) \\ &\quad \times W_1(x, y) W_1(q, p),\end{aligned} \tag{A57}$$

where $W_1(q, p)$ is the WF of the Fock state $|1\rangle$:

$$W_1(q, p) = \frac{1}{2\pi} \exp\left[-\frac{q^2 + p^2}{2}\right](q^2 + p^2 - 1). \tag{A58}$$

The strategy to evaluate the p_{11} contribution of the output state of the gate, given its input state and the physical parameters of the interaction, would be as follows. First, knowing the moments of the input state, we can evaluate the moments of the output state using Eqs. (A50). This allows one to write the WF of the output state. Then, by advantage of Eq. (A57) it is possible to evaluate the p_{11} contribution of the output by integration. The integrand is a polynomial in the integration variables multiplied by a Gaussian kernel, hence the integration is usually possible to carry analytically. The expressions for the case of transformations (A49) corresponding to realistic interaction are, however, very complicated and hardly tractable. In this case, it can be useful to approximate the WF of a single-photon state by a difference of two Gaussian WFs, which allows one to reduce the integration to merely finding determinants of at most 4×4 matrices. This representation technique is inspired by the single-photon generation via the heralded parametric down-conversion [96] and is explained in, e.g., Ref. [93]. We present a more detailed explanation of this technique in Appendix 5.

To find the value of the threshold $F_{11}(\rho)$, we need to evaluate the vacuum contributions of the states of the subsystems. This can be done using relations

$$\begin{aligned}p_{0;a} &= \mathrm{Tr}_b\langle 0_a|\rho|0_a\rangle = \mathrm{Tr}[\rho(|0\rangle\langle 0|_a \otimes \mathbb{1}_b)] \\ &= (4\pi)^2 \int \mathrm{d}x\, \mathrm{d}y\, \mathrm{d}q\, \mathrm{d}p\, W_\rho(x, y, q, p) W_0(x, y),\end{aligned} \tag{A59}$$

where now the variables x, y run over the phase space of the first subsystem. Expression for $p_{0;b}$ can be obtained straightforwardly in an analogous way.

5. Computing the matrix elements using gaussian integrals

First, we present an asymptotic approximation of a single-photon state $|1\rangle$. We start with an expansion of a thermal state in the Fock basis: $\rho_{\mathrm{th}}(n) = \sum_{k=0}^{\infty} p_k |k\rangle\langle k|$, where n is the mean occupation and

$$p_k = \frac{1}{1+n}\left[\frac{n}{1+n}\right]^k. \tag{A60}$$

We consider a state

$$\frac{1}{n}[(1+n)\rho_{\mathrm{th}}(n) - |0\rangle\langle 0|] = |1\rangle\langle 1| + (n+1)\sum_{k=2}^{\infty} p_k |k\rangle\langle k|. \tag{A61}$$

This equation is exact. For low $n \ll 1$, the Fock state contributions p_k decrease approximately as $p_k \propto n^k$, and hence the sum on the right-hand side of the equations above can be approximately ignored. More precisely,

$$|1\rangle\langle 1| = \lim_{n\to 0} \frac{1}{n}[(1+n)\rho_{\mathrm{th}}(n) - |0\rangle\langle 0|]. \tag{A62}$$

This equation allows one to represent the non-Gaussian state $|1\rangle$ as a sum of two Gaussian states, a thermal one, and a vacuum one. Importantly, since the computation of the Wigner function is linear over mixtures of states, that is,

$$W_{\sum_k r_k \rho_k}(x, p) = \sum_k r_k W_{\rho_k}(x, y), \tag{A63}$$

we can represent the Wigner function of $|1\rangle$ as a combination of two Gaussian Wigner functions:

$$\begin{aligned}W_1(x, p) = \lim_{n\to 0} \frac{1}{n}[&(1+n)\mathsf{W}(x, p; \mathbf{0}, (2n+1)\mathbb{1}_2) \\ &- \mathsf{W}(x, p; \mathbf{0}, \mathbb{1}_2)].\end{aligned} \tag{A64}$$

This expression allows us to represent all the states of our interest in the form of combinations of Gaussian Wigner functions. To compute overlaps of such functions, we use the integral relation

$$\begin{aligned}&\int_{\mathbb{R}_n} \mathrm{d}^n\mathbf{X}\ \exp\left\{-\frac{1}{2}\mathbf{X}^T \mathbb{Q}^{-1}\mathbf{X} + i\mathbf{\Lambda}^T\mathbf{X}\right\} \\ &\quad = \sqrt{(2\pi)^n \cdot \det[\mathbb{Q}]}\ \exp\left\{-\frac{1}{2}\mathbf{\Lambda}^T\mathbb{Q}\mathbf{\Lambda}\right\},\end{aligned} \tag{A65}$$

valid for every symmetric real-valued positive-definite matrix $\mathbb{Q}$ of dimensions $n \times n$.

6. Preprocessing input states to produce two-mode squeezing

To compare our result with another approach, we also consider certain nonclassical states. Interestingly, it can be shown that when two independent displaced squeezed states are fed to the input of a unitary QND gate, the output state exhibits properties similar to the TMS state, regarding the value of p_{11} contribution. To observe this, the input states must have the parameters (squeezing angle and magnitude, and displacement) that optimize the value of p_{11} at the output. Notably, after this optimization, the output state can reach the value of $1/4$, which is the maximal value of p_{11} attainable by TMS. We also test the QND gate by simulating a TMS state being fed to the input and optimizing this input state to reach the maximal value of p_{11} at the output. The corresponding state has a trivial maximum at $G = 0$, which corresponds to the TMS state being mapped onto itself, and one additional at $G \approx 2$.

The results of this investigation are illustrated in Fig. 8, where each curve shows the values of the output p_{11} contributions, maximized over the parameters of the input states.

7. Feasibility proof

For the study of the feasibility of our proposed approach, we perform the optimization of the nonclassicality witness Δ using the experimental parameters reported in Ref. [24]. In Ref. [24], the atom-mechanical entanglement is engineered

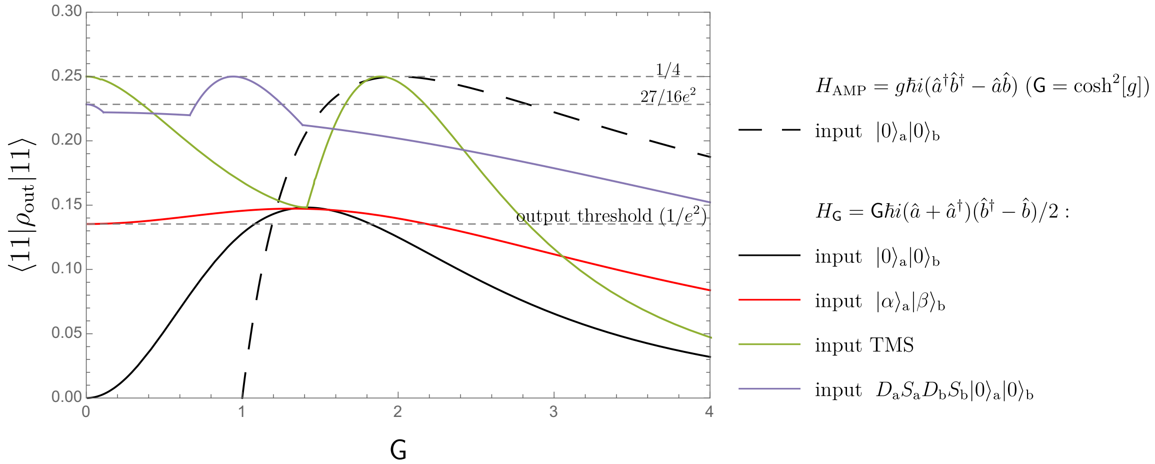

FIG. 8. Comparison of nonclassical coincidences $p_{11} = \langle 11|\rho_{\text{out}}|11\rangle$ generated by TMS and QND interactions. The black dashed line corresponds to the output TMS state. Colored lines to the output generated by the QND interaction from different input states. For each value of gain G, all parameters of input states are optimized to produce maximal p_{11}. The correspondence between the gains of QND and TMS interactions is not direct.

via continuous-drive interaction between atoms and mechanics. Here, using the experimental parameters of Ref. [24] and including the imperfections reported there, we derive the input-output relations for the atom-light gate operated in a pulsed regime and find the optimal nonclassicality witness Δ. The effective Hamiltonian reads (Eq. (B9) in the Supplemental Material of Ref. [24])

$$\hat{H}/\hbar = \frac{\omega_{\text{S}}}{4}\left(\hat{X}_{\text{S}}^2 + \hat{P}_{\text{S}}^2\right) - 2\sqrt{\Gamma_{\text{S}}}(\hat{X}_{\text{S}}\hat{X}_{\text{L}} + \zeta\hat{P}_{\text{S}}\hat{P}_{\text{L}}), \quad \text{(A66)}$$

where the label "S" relates to the atomic (spin) system and "L" to light. Γ_{S} is the coupling rate. The quadratures of the spin oscillator obey $[\hat{X}_{\text{s}}, \hat{P}_{\text{s}}] = 2\text{i}$, the quadratures of light $[\hat{X}_{\text{L}}(t), \hat{P}_{\text{L}}(t')] = 2\text{i}\,\delta(t - t')$ describe the light in a free space. To describe pulsed operation, we need to consider the quadratures of the incident light $(X, P)_{\text{L}}^{\text{in}}$ and the leaking light $(X, P)_{\text{L}}^{\text{out}}$, and define the canonical quadratures of the output light as

$$\hat{\mathbf{X}}_{\text{L}}^{\text{out}} = \frac{1}{\tau}\int_0^\tau \hat{X}_{\text{L}}^{\text{out}}(t), \quad \hat{\mathbf{P}}_{\text{L}}^{\text{out}} = \frac{1}{\tau}\int_0^\tau \hat{P}_{\text{L}}^{\text{out}}(t). \quad \text{(A68)}$$

To write the input-output relations for the quadratures of this system, we need to convert the input-output relations of Ref. [24] [Eqs. (B10) and (B11) in the SM] to the time domain. With notation $X_{\text{S}}(0) = X_{\text{S}}^{\text{in}}$, $X_{\text{S}}(\tau) = X_{\text{S}}^{\text{out}}$ (same for P), the result reads

$$\begin{aligned}\hat{X}_{\text{S}}^{\text{out}} &= M_{1,1}(\tau, 0)\hat{X}_{\text{S}}^{\text{in}} + M_{1,2}(\tau, 0)\hat{P}_{\text{S}}^{\text{in}} \\ &\quad - 2\zeta\sqrt{\Gamma_{\text{S}}}\int_0^\tau M_{1,1}(\tau, s)\hat{P}_{\text{L}}^{\text{in}}(s)\text{d}s \\ &\quad + 2\sqrt{\Gamma_{\text{S}}}\int_0^\tau M_{1,2}(\tau, s)\hat{X}_{\text{L}}^{\text{in}}(s)\text{d}s\,, \end{aligned} \quad \text{(A68)}$$

$$\begin{aligned}\hat{P}_{\text{S}}^{\text{out}} &= M_{1,2}(\tau, 0)\hat{X}_{\text{S}}^{\text{in}} + M_{2,2}(\tau, 0)\hat{P}_{\text{S}}^{\text{in}} \\ &\quad - 2\zeta\sqrt{\Gamma_{\text{S}}}\int_0^\tau M_{1,2}(\tau, s)\hat{P}_{\text{L}}^{\text{in}}(s)\text{d}s \\ &\quad + 2\sqrt{\Gamma_{\text{S}}}\int_0^\tau M_{2,2}(\tau, s)\hat{X}_{\text{L}}^{\text{in}}(s)\text{d}s\,, \end{aligned} \quad \text{(A69)}$$

$$\begin{aligned}\hat{\mathbf{X}}_{\text{L}}^{\text{out}} &= -\zeta\frac{\sqrt{\Gamma_{\text{S}}}}{\tau}\int_0^\tau M_{2,1}(\tau', 0)\text{d}\tau' \times \hat{X}_{\text{S}}^{\text{in}} \\ &\quad - \zeta\frac{\sqrt{\Gamma_{\text{S}}}}{\tau}\int_0^\tau M_{2,2}(\tau', 0)\text{d}\tau' \times \hat{P}_{\text{S}}^{\text{in}} \\ &\quad + \frac{1}{\tau}\int_0^\tau \text{d}\tau'\,\hat{X}_{\text{L}}^{\text{in}}(\tau')\left(1 - 2\Gamma_{\text{S}}\zeta\int_{\tau'}^\tau M_{2,2}(s, \tau')\text{d}s\right) \\ &\quad + \frac{2\Gamma_{\text{S}}\zeta^2}{\tau}\int_0^\tau \text{d}\tau'\int_0^{\tau'} M_{2,1}(\tau', s)\hat{P}_{\text{L}}^{\text{in}}(s)\text{d}s\,, \end{aligned} \quad \text{(A70)}$$

$$\begin{aligned}\hat{\mathbf{P}}_{\text{L}}^{\text{out}} &= \frac{\sqrt{\Gamma_{\text{S}}}}{\tau}\int_0^\tau M_{1,1}(\tau', 0)\text{d}\tau' \times \hat{X}_{\text{S}}^{\text{in}} \\ &\quad + \frac{\sqrt{\Gamma_{\text{S}}}}{\tau}\int_0^\tau M_{1,2}(\tau', 0)\text{d}\tau' \times \hat{P}_{\text{S}}^{\text{in}} \\ &\quad + \frac{2\Gamma_{\text{S}}}{\tau}\int_0^\tau \text{d}\tau'\int_0^{\tau'} M_{1,2}(\tau', s)\hat{X}_{\text{L}}^{\text{in}}(s)\text{d}s + \frac{1}{\tau}\int_0^\tau \text{d}\tau' \\ &\quad \times \hat{P}_{\text{L}}^{\text{in}}(\tau')\left(1 - 2\Gamma_{\text{S}}\zeta\int_{\tau'}^\tau M_{1,1}(s, \tau')\text{d}s\right), \end{aligned} \quad \text{(A71)}$$

where

$$\begin{aligned} M(\tau, s) &= \exp\left[\frac{1}{2}(\gamma + 2\Gamma_{\text{S}}\zeta)(\tau - s)\right] \\ &\quad \times \begin{pmatrix} \cos[(s - \tau)\omega_{\text{s}}] & \sin[(s - \tau)\omega_{\text{s}}] \\ -\sin[(s - \tau)\omega_{\text{s}}] & \cos[(s - \tau)\omega_{\text{s}}] \end{pmatrix}. \end{aligned} \quad \text{(A72)}$$

Here γ is the linewidth of the atomic oscillator.

Equation (A71) is sufficient to reconstruct the output atom-light state, so we can calculate $\langle 11|\rho_{\text{out}}|11\rangle$, $F_{11}(\rho_{\text{out}})$ and find the nonclassicality Δ. In Fig. 9, we show $\langle 11|\rho_{\text{out}}|11\rangle$ and $F_{11}(\rho_{\text{out}})$ as a function of the pulse duration τ. We make the

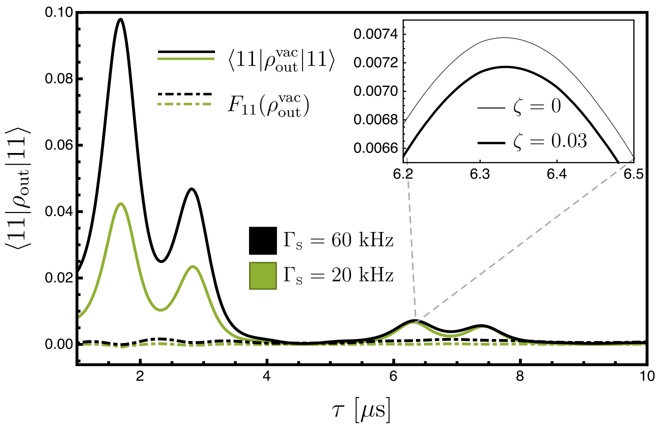

FIG. 9. Nonclassical coincidences $\langle 11|\rho_{\rm out}|11\rangle$ (solid curves) and nonclassicality thresholds $F_{11}(\rho_{\rm out})$ (dot-dashed curves) calculated for the output state of an atom-light QND gate with a vacuum input. Color codes the readout rate Γ_s (green from Ref. [24] and black for Ref. [22]). In certain regions, the p_{11} contribution significantly prevails over the threshold. The difference caused by the back-action terms is negligible (see inset for a magnified region). Other parameters used for simulations are $\gamma = 2\pi \times 1.7$ kHz, $\omega_s = 2\pi \times 1.37$ MHz.

estimations for two values of the coupling rate $\Gamma_S = 20$ kHz directly taken from Ref. [24], and another one ($\Gamma_S = 60$ kHz) from a previous work by the same group [22]. The estimations show that already with feasible parameters it is possible to generate nonclassical coincidences of photons and collective spin excitations. For both coupling rates, we made estimations without ($\zeta = 0$) and with ($\zeta \neq 0$) the back-action terms. As follows from Fig. 9, the difference caused by the back-action terms is negligible.

8. Experimental parameters vs calculation

In this paper, we use dimensionless parameters of the atom-light, mechanical-light, and atom-mechanical QND gates, scaling all of them in the units of κ_m, the damping rate of the optomechanical cavity. To prove that numbers used in our calculations belong to a feasible region, we compare the most important of them to the corresponding parameters of Refs. [23,24] (see Table I) as well scaled to κ_m.

TABLE I. Parameters of Refs. [23,24], both in dimensional units and scaled to the linewidth of the optomechanical cavity κ_m, compared to the ones used in the calculations (simulation). Here, $g_{a,m}$ are the coupling strengths of the atom-light and optomechanical QND interactions, $\Gamma_m = \gamma_m n_{th}$ is the mechanical thermalization rate derived from mechanical linewidth γ_m and mean thermal occupation of the mechanical environment n_{th}. Parameter g_a for Refs. [23,24] is recalculated for the atom-light interaction inside a cavity using the original values of the coupling between atoms and free-space light.

			Scaled to κ_m		
Parameter	[24]	[23]	[24]	[23]	Simulation
$\kappa_m/2\pi$	2.1MHz	31.5MHz	1	1	1
$g_m/2\pi$	0.35MHz	0.97MHz	0.17	0.03	0.05–0.07
$\Gamma_m/2\pi$	363.3Hz	22.58kHz	10^{-3}	7×10^{-4}	$10^{-5} - 10^{-2}$
$g_a/2\pi$	0.25MHz	0.08MHz	0.07	0.003	0.05–0.07

Rethermalization rate [$\Gamma_m = \gamma_m(n_{th}^{mech} + 1/2)$] and the coupling constant of the optomechanical interaction g_m are exactly what is measured in Refs. [23,24], so they can be compared directly. The coupling constant g_a of the atom-light QND interaction should be recalculated since there are no cavities used for the atomic subsystems in either reference. The QND part of the effective Hamiltonian of the atom-light interaction in free space is $\hat{H} = \sqrt{\Gamma_s}\hat{X}_s(t)\hat{X}_a$, where $\hat{X}_s(t)$ corresponds to the light mode in a free space and dimensionless $\hat{X}_a$ is the canonical quadrature corresponding to the spin subsystem. The interaction establishes a QND gate between canonical variables $\hat{X}_a$ and $\frac{1}{\sqrt{\tau}}\int_0^\tau \hat{X}_s(t)dt$, and such a gate is characterized by dimensionless gain G_1. If we place atoms in the cavity (with the damping rate κ_m) and consider the similar intracavity interaction $\hat{H} = g_a\hat{X}_l\hat{X}_a$, where $\hat{X}_l$ is a dimensionless quadrature of the cavity light mode, we would have the similar QND gate between canonical variables $\hat{X}_a$ and $\frac{1}{\sqrt{\tau}}\int_0^\tau \hat{X}_{out}(t)dt$, where $\hat{X}_{out}$ corresponds to the output light pulse (free space). This gate is characterized by dimensionless gain $G_2 = g_a\sqrt{2\tau/\kappa_m}$. Assuming $G_1 = G_2$, we can evaluate g_a via Γ_s.

[1] G. Kurizki, P. Bertet, Y. Kubo, K. Mølmer, D. Petrosyan, P. Rabl, and J. Schmiedmayer, Quantum technologies with hybrid systems, Proc. Natl. Acad. Sci. USA **112**, 3866 (2015).

[2] D. Lee, K. W. Lee, J. V. Cady, P. Ovartchaiyapong, and A. C. Bleszynski Jayich, Topical review: Spins and mechanics in diamond, J. Opt. **19**, 033001 (2017).

[3] A. A. Clerk, K. W. Lehnert, P. Bertet, J. R. Petta, and Y. Nakamura, Hybrid quantum systems with circuit quantum electrodynamics, Nat. Phys. **16**, 257 (2020).

[4] P. van Loock, Optical hybrid approaches to quantum information, Laser Photonics Rev. **5**, 167 (2011).

[5] U. L. Andersen, J. S. Neergaard-Nielsen, P. van Loock, and A. Furusawa, Hybrid discrete- and continuous-variable quantum information, Nat. Phys. **11**, 713 (2015).

[6] Edward Uhler Condon and H. Odabasl, *Atomic Structure* (Cambridge University Press, Cambridge, 2010).

[7] C. Cohen-Tannoudji, J. Dupont-Roc, and G. Grynberg, *Atom-Photon Interactions: Basic Processes and Applications* (Wiley, New York, 1998).

[8] Q. Glorieux, T. Aladjidi, P. D. Lett, and R. Kaiser, Hot atomic vapors for nonlinear and quantum optics, New J. Phys. **25**, 051201 (2023).

[9] A. N. Cleland, *Foundations of Nanomechanics: From Solid-State Theory to Device Applications* (Springer Science & Business Media, Berlin, Germany, 2013).

[10] M. Šiler, L. Ornigotti, O. Brzobohatý, P. Jákl, A. Ryabov, V. Holubec, P. Zemánek, and R. Filip, Diffusing up the hill: Dynamics and equipartition in highly unstable systems, Phys. Rev. Lett. **121**, 230601 (2018).

[11] P. Treutlein, C. Genes, K. Hammerer, M. Poggio, and P. Rabl, Hybrid Mechanical Systems, in *Cavity Optomechanics: Nano- and Micromechanical Resonators Interacting with Light*, edited by M. Aspelmeyer, T. J. Kippenberg, and F. Marquardt (Springer, Berlin, 2014), pp. 327–351.

[12] A. Välimaa, W. Crump, M. Kervinen, and M. A. Sillanpää, Multiphonon transitions in a quantum electromechanical system, Phys. Rev. Appl. **17**, 064003 (2022).

[13] J. Kettler, N. Vaish, Laure Mercier de Lépinay, B. Besga, Pierre-Louis de Assis, O. Bourgeois, A. Auffèves, M. Richard, J. Claudon, J.-M. Gérard, B. Pigeau, O. Arcizet, P. Verlot, and Jean-Philippe Poizat, Inducing micromechanical motion by optical excitation of a single quantum dot, Nat. Nanotechnol. **16**, 283 (2021).

[14] J. V. Cady, O. Michel, K. W. Lee, R. N. Patel, C. J. Sarabalis, A. H. Safavi-Naeini, and A. C. Bleszynski Jayich, Diamond optomechanical crystals with embedded nitrogen-vacancy centers, Quantum Sci. Technol. **4**, 024009 (2019).

[15] J.-M. Pirkkalainen, S. U. Cho, J. Li, G. S. Paraoanu, P. J. Hakonen, and M. A. Sillanpää, Hybrid circuit cavity quantum electrodynamics with a micromechanical resonator, Nature (London) **494**, 211 (2013).

[16] R. D. Delaney, M. D. Urmey, S. Mittal, B. M. Brubaker, J. M. Kindem, P. S. Burns, C. A. Regal, and K. W. Lehnert, Superconducting-qubit readout via low-backaction electro-optic transduction, Nature (London) **606**, 489 (2022).

[17] H. J. Kimble, The quantum internet, Nature (London) **453**, 1023 (2008).

[18] Georgi Gary Rozenman, Neel Kanth Kundu, R. Liu, L. Zhang, A. Maslennikov, Y. Reches, and Heung Youl Youm, The quantum internet: A synergy of quantum information technologies and 6G networks, IET Quantum Commun. **4**, 147 (2023).

[19] K. Hammerer, M. Aspelmeyer, E. S. Polzik, and P. Zoller, Establishing Einstein-Poldosky-Rosen channels between nanomechanics and atomic ensembles, Phys. Rev. Lett. **102**, 020501 (2009).

[20] S. Camerer, M. Korppi, A. Jöckel, D. Hunger, T. W. Hänsch, and P. Treutlein, Realization of an optomechanical interface between ultracold atoms and a membrane, Phys. Rev. Lett. **107**, 223001 (2011).

[21] A. Jöckel, A. Faber, T. Kampschulte, M. Korppi, M. T. Rakher, and P. Treutlein, Sympathetic cooling of a membrane oscillator in a hybrid mechanical-atomic system, Nat. Nanotechnol. **10**, 55 (2015).

[22] C. B. Møller, R. A. Thomas, G. Vasilakis, E. Zeuthen, Y. Tsaturyan, M. Balabas, K. Jensen, A. Schliesser, K. Hammerer, and E. S. Polzik, Quantum back-action-evading measurement of motion in a negative mass reference frame, Nature (London) **547**, 191 (2017).

[23] T. M. Karg, B. Gouraud, Chun Tat Ngai, Gian-Luca Schmid, K. Hammerer, and P. Treutlein, Light-mediated strong coupling between a mechanical oscillator and atomic spins 1 meter apart, Science **369**, 174 (2020).

[24] R. A. Thomas, Michał Parniak, C. Østfeldt, C. B. Møller, C. Bærentsen, Y. Tsaturyan, A. Schliesser, Jürgen Appel, E. Zeuthen, and E. S. Polzik, Entanglement between distant macroscopic mechanical and spin systems, Nat. Phys. **17**, 228 (2021).

[25] V. B. Braginsky, Y. I. Vorontsov, and K. S. Thorne, Quantum nondemolition measurements, Science **209**, 547 (1980).

[26] P. Grangier, Juan Ariel Levenson, and Jean-Philippe Poizat, Quantum non-demolition measurements in optics, Nature (London) **396**, 537 (1998).

[27] R. Filip, Continuous-variable quantum erasing, Phys. Rev. A **67**, 042111 (2003).

[28] R. Filip, Continuous-variable quantum nondemolishing interaction at a distance, Phys. Rev. A **69**, 052313 (2004).

[29] L. Mišta and R. Filip, Quantum nondemolition measurement saturates fidelity trade-off, Phys. Rev. A **72**, 034307 (2005).

[30] L. Mišta and R. Filip, Improving teleportation of continuous variables by local operations, Phys. Rev. A **71**, 032342 (2005).

[31] N. C. Menicucci, P. van Loock, M. Gu, C. Weedbrook, T. C. Ralph, and M. A. Nielsen, Universal quantum computation with continuous-variable cluster states, Phys. Rev. Lett. **97**, 110501 (2006).

[32] R. Filip, Excess-noise-free recording and uploading of nonclassical states to continuous-variable quantum memory, Phys. Rev. A **78**, 012329 (2008).

[33] Y. Miwa, R. Ukai, Jun-Ichi Yoshikawa, R. Filip, P. van Loock, and A. Furusawa, Demonstration of cluster-state shaping and quantum erasure for continuous variables, Phys. Rev. A **82**, 032305 (2010).

[34] S. Yokoyama, R. Ukai, Jun-ichi Yoshikawa, P. Marek, R. Filip, and A. Furusawa, Nonlocal quantum gate on quantum continuous variables with minimal resources, Phys. Rev. A **90**, 012311 (2014).

[35] Vojtěch Kupčík and R. Filip, Continuous-variable entanglement mediated by a thermal oscillator, Phys. Rev. A **92**, 022346 (2015).

[36] A. D. Manukhova, A. A. Rakhubovsky, and R. Filip, Pulsed atom-mechanical quantum non-demolition gate, npj Quantum Inf. **6**, 4 (2020).

[37] A. D. Manukhova, A. A. Rakhubovsky, and R. Filip, Atom-mechanical Hong-Ou-Mandel interference, Quantum **6**, 686 (2022).

[38] A. Heidmann, R. J. Horowicz, S. Reynaud, E. Giacobino, C. Fabre, and G. Camy, Observation of quantum noise reduction on twin laser beams, Phys. Rev. Lett. **59**, 2555 (1987).

[39] J. F. Clauser, Experimental distinction between the quantum and classical field-theoretic predictions for the photoelectric effect, Phys. Rev. D **9**, 853 (1974).

[40] P. Kolchin, S. Du, C. Belthangady, G. Y. Yin, and S. E. Harris, Generation of narrow-bandwidth paired photons: Use of a single driving laser, Phys. Rev. Lett. **97**, 113602 (2006).

[41] J. K. Thompson, J. Simon, H. Loh, and V. Vuletić, A high-brightness source of narrowband, identical-photon pairs, Science **313**, 74 (2006).

[42] A. Kuzmich, W. P. Bowen, A. D. Boozer, A. Boca, C. W. Chou, L.-M. Duan, and H. J. Kimble, Generation of nonclassical photon pairs for scalable quantum communication with atomic ensembles, Nature (London) **423**, 731 (2003).

[43] R. Riedinger, S. Hong, R. A. Norte, J. A. Slater, J. Shang, A. G. Krause, V. Anant, M. Aspelmeyer, and S. Gröblacher, Non-classical correlations between single photons and phonons from a mechanical oscillator, Nature (London) **530**, 313 (2016).

[44] M. Zugenmaier, K. B. Dideriksen, A. S. Sørensen, B. Albrecht, and E. S. Polzik, Long-lived non-classical correlations towards quantum communication at room temperature, Commun. Phys. **1**, 76 (2018).

[45] E. Bimbard, R. Boddeda, N. Vitrant, A. Grankin, V. Parigi, J. Stanojevic, A. Ourjoumtsev, and P. Grangier, Homodyne tomography of a single photon retrieved on demand from a cavity-enhanced cold atom memory, Phys. Rev. Lett. **112**, 033601 (2014).
[46] P Jobez, I Usmani, N Timoney, C Laplane, N Gisin, and M Afzelius, Cavity-enhanced storage in an optical spin-wave memory, New J. Phys. **16**, 083005 (2014).
[47] D. J. Saunders, J. H. D. Munns, T. F. M. Champion, C. Qiu, K. T. Kaczmarek, E. Poem, P. M. Ledingham, I. A. Walmsley, and J. Nunn, Cavity-enhanced room-temperature broadband raman memory, Phys. Rev. Lett. **116**, 090501 (2016).
[48] V. V. Kuz'min, A. N. Vetlugin, and I. V. Sokolov, Control of parameters of quantum memory for light in a cavity configuration, Opt. Spectrosc. **119**, 1004 (2015).
[49] N. G. Veselkova, N. I. Masalaeva, and I. V. Sokolov, Cavity-assisted atomic raman memories beyond the bad cavity limit: Effect of four-wave mixing, Phys. Rev. A **99**, 013814 (2019).
[50] N J Cerf, G Leuchs, and E S Polzik, *Quantum Information with Continuous Variables of Atoms and Light* (Imperial College Press, London, UK, 2007).
[51] M. Aspelmeyer, T. J. Kippenberg, and F. Marquardt, Cavity optomechanics, Rev. Mod. Phys. **86**, 1391 (2014).
[52] R. El-Ganainy, M. Khajavikhan, D. N. Christodoulides, and S. K. Ozdemir, The dawn of non-Hermitian optics, Commun. Phys. **2**, 37 (2019).
[53] C. Wang, Z. Fu, W. Mao, J. Qie, A. D. Stone, and L. Yang, Non-Hermitian optics and photonics: From classical to quantum, Adv. Opti. Photon. **15**, 442 (2023).
[54] K. Makino, Y. Hashimoto, Jun-ichi Yoshikawa, H. Ohdan, T. Toyama, P. van Loock, and A. Furusawa, Synchronization of optical photons for quantum information processing, Sci. Adv. **2**, e1501772 (2016).
[55] K. Hammerer, A. S. Sørensen, and E. S. Polzik, Quantum interface between light and atomic ensembles, Rev. Mod. Phys. **82**, 1041 (2010).
[56] M. R. Vanner, I. Pikovski, and M. S. Kim, Towards optomechanical quantum state reconstruction of mechanical motion, Ann. Phys. **527**, 15 (2015).
[57] L. Mandel and E. Wolf, *Optical Coherence and Quantum Optics* (Cambridge University Press, Cambridge, 1995).
[58] W. Vogel and Dirk-Gunnar Welsch, *Quantum Optics* (John Wiley & Sons, Weinheim, Germany, 2006).
[59] D. N. Klyshko, The nonclassical light, Phys. Usp. **39**, 573 (1996).
[60] Th. Richter and W. Vogel, Nonclassicality of quantum states: A hierarchy of observable conditions, Phys. Rev. Lett. **89**, 283601 (2002).
[61] A. Mari and J. Eisert, Positive Wigner functions render classical simulation of quantum computation efficient, Phys. Rev. Lett. **109**, 230503 (2012).
[62] J. Kohler, J. A. Gerber, E. Dowd, and D. M. Stamper-Kurn, Negative-mass instability of the spin and motion of an atomic gas driven by optical cavity backaction, Phys. Rev. Lett. **120**, 013601 (2018).
[63] L. Qiu, I. Shomroni, P. Seidler, and T. J. Kippenberg, Laser cooling of a nanomechanical oscillator to its zero-point energy, Phys. Rev. Lett. **124**, 173601 (2020).
[64] L. M. de Lépinay, C. F. Ockeloen-Korppi, M. J. Woolley, and M. A. Sillanpää, Quantum mechanics–free subsystem with mechanical oscillators, Science **372**, 625 (2021).
[65] C. U. Lei, A. J. Weinstein, J. Suh, E. E. Wollman, A. Kronwald, F. Marquardt, A. A. Clerk, and K. C. Schwab, Quantum nondemolition measurement of a quantum squeezed state beyond the 3 dB limit, Phys. Rev. Lett. **117**, 100801 (2016).
[66] C. F. Ockeloen-Korppi, E. Damskägg, J.-M. Pirkkalainen, A. A. Clerk, M. J. Woolley, and M. A. Sillanpää, Quantum backaction evading measurement of collective mechanical modes, Phys. Rev. Lett. **117**, 140401 (2016).
[67] I. Shomroni, L. Qiu, D. Malz, A. Nunnenkamp, and T. J. Kippenberg, Optical backaction-evading measurement of a mechanical oscillator, Nat. Commun. **10**, 2086 (2019).
[68] Y. Liu, J. Zhou, L. M. de Lépinay, and M. A. Sillanpää, Quantum backaction evading measurements of a silicon nitride membrane resonator, New J. Phys. **24**, 083043 (2022).
[69] Y. Chu and S. Gröblacher, A perspective on hybrid quantum opto- and electromechanical systems, Appl. Phys. Lett. **117**, 150503 (2020).
[70] F. Y. Khalili and E. S. Polzik, Overcoming the standard quantum limit in gravitational wave detectors using spin systems with a negative effective mass, Phys. Rev. Lett. **121**, 031101 (2018).
[71] E. Zeuthen, E. S. Polzik, and Farid Ya Khalili, Gravitational wave detection beyond the standard quantum limit using a negative-mass spin system and virtual rigidity, Phys. Rev. D **100**, 062004 (2019).
[72] E. Zeuthen, E. S. Polzik, and Farid Ya. Khalili, Trajectories without quantum uncertainties in composite systems with disparate energy spectra, PRX Quantum **3**, 020362 (2022).
[73] D. N. Matsukevich, T. Chanelière, S. D. Jenkins, S.-Y. Lan, T. A. B. Kennedy, and A. Kuzmich, Entanglement of remote atomic qubits, Phys. Rev. Lett. **96**, 030405 (2006).
[74] I. Straka, A. Predojević, T. Huber, L. Lachman, L. Butschek, M. Miková, M. Mičuda, G. S. Solomon, G. Weihs, M. Ježek, and R. Filip, Quantum non-Gaussian depth of single-photon states, Phys. Rev. Lett. **113**, 223603 (2014).
[75] A. I. Lvovsky, H. Hansen, T. Aichele, O. Benson, J. Mlynek, and S. Schiller, Quantum state reconstruction of the single-photon Fock state, Phys. Rev. Lett. **87**, 050402 (2001).
[76] E. Bimbard, N. Jain, A. MacRae, and A. I. Lvovsky, Quantum-optical state engineering up to the two-photon level, Nat. Photonics **4**, 243 (2010).
[77] C. W. Chou, H. de Riedmatten, D. Felinto, S. V. Polyakov, S. J. van Enk, and H. J. Kimble, Measurement-induced entanglement for excitation stored in remote atomic ensembles, Nature (London) **438**, 828 (2005).
[78] R. Riedinger, A. Wallucks, I. Marinković, C. Löschnauer, M. Aspelmeyer, S. Hong, and S. Gröblacher, Remote quantum entanglement between two micromechanical oscillators, Nature (London) **556**, 473 (2018).
[79] A. Wallucks, I. Marinković, B. Hensen, R. Stockill, and S. Gröblacher, A quantum memory at telecom wavelengths, Nat. Phys. **16**, 772 (2020).
[80] D. Felinto, C. W. Chou, J. Laurat, E. W. Schomburg, H. de Riedmatten, and H. J. Kimble, Conditional control of the quantum states of remote atomic memories for quantum networking, Nat. Phys. **2**, 844 (2006).

[81] R. N. Patel, T. P. McKenna, Z. Wang, J. D. Witmer, W. Jiang, R. Van Laer, C. J. Sarabalis, and A. H. Safavi-Naeini, Room-temperature mechanical resonator with a single added or subtracted phonon, Phys. Rev. Lett. **127**, 133602 (2021).

[82] G. Enzian, L. Freisem, J. J. Price, A. Ø. Svela, J. Clarke, B. Shajilal, J. Janousek, B. C. Buchler, P. K. Lam, and M. R. Vanner, Non-Gaussian mechanical motion via single and multi-phonon subtraction from a thermal state, Phys. Rev. Lett. **127**, 243601 (2021).

[83] Y. S. S. Patil, J. Yu, S. Frazier, Y. Wang, K. Johnson, J. Fox, J. Reichel, and J. G. E. Harris, Measuring high-order phonon correlations in an optomechanical resonator, Phys. Rev. Lett. **128**, 183601 (2022).

[84] M. Walschaers, Non-Gaussian quantum states and where to find them, PRX Quantum **2**, 030204 (2021).

[85] L. Lachman and R. Filip, Quantum non-Gaussianity of light and atoms, Prog. Quantum Electron. **83**, 100395 (2022).

[86] L. Pezzè, A. Smerzi, M. K. Oberthaler, R. Schmied, and P. Treutlein, Quantum metrology with nonclassical states of atomic ensembles, Rev. Mod. Phys. **90**, 035005 (2018).

[87] A. A. Rakhubovsky, D. W. Moore, and R. Filip, Quantum non-Gaussian optomechanics and electromechanics, Prog. Quantum Electron. **93**, 100495 (2024).

[88] F. Wolf, C. Shi, J. C. Heip, M. Gessner, L. Pezzè, A. Smerzi, M. Schulte, K. Hammerer, and P. O. Schmidt, Motional Fock states for quantum-enhanced amplitude and phase measurements with trapped ions, Nat. Commun. **10**, 1 (2019).

[89] A. A. Rakhubovsky and R. Filip, Stroboscopic high-order nonlinearity for quantum optomechanics, npj Quantum Inf. **7**, 120 (2021).

[90] H. Ren, T. Shah, H. Pfeifer, C. Brendel, V. Peano, F. Marquardt, and O. Painter, Topological phonon transport in an optomechanical system, Nat. Commun. **13**, 3476 (2022).

[91] B. Simon, *Trace Ideals and Their Applications*, 2nd ed. (American Mathematical Society, Providence, RI, 2010).

[92] C. Weedbrook, S. Pirandola, R. García-Patrón, N. J. Cerf, T. C. Ralph, J. H. Shapiro, and S. Lloyd, Gaussian quantum information, Rev. Mod. Phys. **84**, 621 (2012).

[93] C. Navarrete-Benlloch, *An Introduction to the Formalism of Quantum Information with Continuous Variables* (Morgan & Claypool Publishers, San Rafael, CA, 2015), pp. 2053-2571.

[94] W. P. Schleich, *Quantum Optics in Phase Space*, 1st ed. (Wiley-VCH, Berlin, 2001).

[95] J. Weinbub and D. K. Ferry, Recent advances in Wigner function approaches, Appl. Phys. Rev. **5**, 041104 (2018).

[96] T. Aichele, A. I. Lvovsky, and S. Schiller, Optical mode characterization of single photons prepared via conditional measurements on a biphoton state, Eur. Phys. J. D **18**, 237 (2002).